

SHEDDING LIGHT ON DARK SATELLITES



SHEDDING LIGHT ON DARK SATELLITES

By

SARAH LOUISE NICKERSON, B.Sc.

A Thesis

Submitted to the School of Graduate Studies

in Partial Fulfilment of the Requirements

for the Degree

Master of Science

McMaster University

©Copyright by Sarah Nickerson, August 2010

MASTER OF SCIENCE (2010)  
(Physics and Astronomy)

McMaster University  
Hamilton, Ontario

TITLE: Shedding Light on Dark Satellites

AUTHOR: Sarah Nickerson, B.Sc. (University of Toronto)

SUPERVISOR: Hugh Couchman

NUMBER OF PAGES: x, 83

# Abstract

We present a study of satellites in orbit around high-resolution, smoothed particle hydrodynamics (SPH) galaxies simulated in cosmological contexts. For the galaxies of similar mass to the Milky Way, the luminosity function at redshift zero of the satellites is similar to the observed luminosity function of the system of satellites orbiting the Milky Way. Analysis of the satellites' mass functions reveals an order of magnitude more dark satellites than luminous for each galaxy. There are even *dark* subhalos more massive than some of the luminous subhalos. What separates luminous and dark subhalos is not their mass at  $z = 0$ , but the maximum mass a subhalo attained over their life. We study the effect of four mass-loss mechanisms on the subhalos: ultraviolet (UV) ionising radiation, tidal stripping, ram pressure stripping, and stellar feedback, and compare the impact each have on the satellites. In the lowest mass subhalos, UV is responsible for most of the gas loss and ram pressure stripping removes the rest. More massive subhalos have deeper potential wells and retain more mass during reionisation. However, as satellites pass near the centre of their main halo, tidal forces cause mass loss from satellites of all masses. It is difficult to discriminate mass loss due to this stellar feedback from other mechanisms using our analysis. During the course of this analysis, we noticed that massive and highly luminous subhalos accrete gas in a region that extends beyond their origins and traces their orbit around the host halo. We also ran a second series of tests by varying the baryonic physics for a smaller galaxy and found that stellar feedback and UV ionisation do have a profound effect of the subhalos.

# Acknowledgements

I would like to graciously thank Greg Stinson, Hugh Couchman, Jeremy Bailin, and James Wadsley for creating the MUGS simulations, and for their many invaluable conversations, feedback, assistance and critique without which this research would not exist. Also, SHARCNET provided supercomputers, and NSERC funding for this project to happen. Alana Krider helped with the formatting of this thesis.

# Table of Contents

Descriptive Notes	ii
Abstract	iii
Acknowledgements	iv
List of Figures	vii
List of Tables	x
<b>Chapter 1 Introduction</b>	<b>1</b>
1.1 $\Lambda$ Cold Dark Matter . . . . .	1
1.2 The Missing Satellites Problem . . . . .	4
1.3 Solving the Missing Satellites Problem: Mechanisms for Baryon Removal . . . . .	6
1.4 Dwarf Galaxies . . . . .	9
1.5 Outline . . . . .	10
<b>Chapter 2 Method</b>	<b>13</b>
2.1 MUGS: The McMaster Unbiased Galaxy Simulations . . . . .	13
2.2 Group Finding: Amiga Halo Finder . . . . .	15
2.3 Merger Trees . . . . .	16
2.4 The Fourteen MUGS Galaxies . . . . .	17
<b>Chapter 3 Simulated Luminosity Functions</b>	<b>19</b>

3.1	Fourteen Systems of Satellites . . . . .	19
3.2	Effects of Stellar Feedback and Ultraviolet Background: g5664 . . . . .	26
<b>Chapter 4 Gas Loss Mechanisms Through Satellite Histories: g15784</b>		
	<b>in Depth</b>	<b>31</b>
4.1	Ultraviolet Background . . . . .	37
4.2	Tidal Stripping . . . . .	43
4.3	Ram Pressure Stripping . . . . .	44
4.4	Stellar Feedback . . . . .	50
4.5	A Combination of Mechanisms . . . . .	52
4.6	Baryon Excess in Massive Halos . . . . .	59
<b>Chapter 5 The Cutoff Between Luminous and Dark Satellites</b>		<b>65</b>
<b>Chapter 6 Conclusions and Discussion</b>		<b>71</b>

# List of Figures

3.1	Cumulative V-band luminosity functions of the subhalo populations of the host galaxies at $z = 0$ . . . . .	22
3.2	Baryon mass versus total mass for subhalo populations at redshift zero . . . . .	24
3.3	Baryon mass versus total mass for the subhalo population of g15784	25
3.4	Cumulative mass function for the subhalo population of each galaxy at $z = 0$ . . . . .	27
3.5	Cumulative luminosity function for g5664, comparing runs with three different conditions on the baryonic physics . . . . .	29
3.6	Cumulative mass function for g5664, comparing runs with three different conditions on the baryonic physics . . . . .	30
4.1	The time evolution of the distance to the host and the mass of three massive, luminous subhalos in g15784 . . . . .	33
4.2	The time evolution of the distance to the host and the mass of three medium to low mass subhalos in g15784 that have formed stars	34
4.3	The time evolution of the distance to the host and the mass of three medium to low mass subhalos in g15784 that have never formed stars . . . . .	35
4.4	$T_{background}$ and $T_{vir}$ over time for two subhalos in g15784 . . . . .	41

4.5	The baryon fraction verses the maximum ratio between the virial and background gas temperatures that a subhalo ever obtains over its lifetime for all subhalos in g15784 . . . . .	42
4.6	Tidal stripping removing gas from a $2.0 \times 10^8 M_{\odot}$ subhalo between redshift 1.0 and 0.8 . . . . .	45
4.7	The gas temperature and density profile of g15784 . . . . .	47
4.8	Ram pressure stripping removing gas from a $1.7 \times 10^9 M_{\odot}$ subhalo between redshift 0.26 and 0.16. . . . .	49
4.9	Pressure versus time for two subhalos . . . . .	50
4.10	Mechanisms for baryon loss over time for a massive subhalo . . .	54
4.11	Mechanisms for baryon loss over time for a massive subhalo . . .	54
4.12	Mechanisms for baryon loss over time for a massive subhalo . . .	55
4.13	Mechanisms for baryon loss over time for a luminous medium mass subhalo . . . . .	55
4.14	Mechanisms for baryon loss over time for a luminous low mass subhalo	56
4.15	Mechanisms for baryon loss over time for a dark low mass subhalo	56
4.16	Mechanisms for baryon loss over time for a medium mass dark subhalo	57
4.17	Mechanisms for baryon loss over time for a medium mass dark subhalo	57
4.18	Mechanisms for baryon loss over time for a low mass dark subhalo	58
4.19	Mechanisms for baryon loss at $z = 0$ for all subhalos in g15784 . .	60

4.20	Time evolution of a luminous subhalo's mass, broken down into particle type and if present at time of maximum mass or not . . . . .	61
4.21	Snapshots at redshift 6 of two subhalos and the non-twin gas they will absorb . . . . .	63
5.1	The baryon fraction at redshift zero divided by the maximum mass versus the subhalos' maximum mass, for six MUGS galaxies . . . . .	68
5.2	The subhalos' maximum mass verses their mass at redshift zero, for six MUGS galaxies . . . . .	69
5.3	For the subhalo population of g15784, the ratio of maximum mass to final mass, verses the minimum distance to the host. . . . .	70

# List of Tables

2.1	The attributes of the fourteen MUGS galaxies . . . . .	18
4.1	The mass at redshift zero and the maximum mass ever achieved over time for nine subhalos in g15784 . . . . .	36
5.1	The highest maximum mass a dark satellite ever has, and the lowest maximum mass a luminous satellites ever has for six MUGS galaxies . . . . .	67

# Chapter 1

## Introduction

### 1.1 $\Lambda$ Cold Dark Matter

The most widely-accepted cosmology model is  $\Lambda$  Cold Dark Matter ( $\Lambda$ CDM) (Ratra & Vogeley, 2008). The  $\Lambda$  in  $\Lambda$ CDM refers to the presence of a non-zero cosmological constant (Gramann, 1988) in the Friedman equations (Friedman, 1922) that describe the expansion of space. The CDM refers to the matter that composes most of the Universe, which is dark (does not interact with electromagnetic radiation) and is cold (non-relativistic).

Dark matter first arose out of a need to explain the measured internal velocities of galaxies in clusters (e.g. Zwicky, 1933; Smith, 1936), galaxies (e.g. Babcock, 1939; Oort, 1940) and the rotation curves of galaxies (Rubin et al., 1978), which were too high for the mass of luminous matter that they held. In order for these results to be consistent with Newtonian mechanics and gravity, unseen matter embedded within the massive halos of galaxies had to be invoked (Einasto et al., 1974; Ostriker et al., 1974).

There is a second motivation for dark matter. For Big Bang inflationary models of the Universe, radiation and matter are coupled during the hot radiation-dominated era (Gamow, 1948) until they become decoupled during recombination. However, after recombination in order for structure to arise from gravitational instabilities in density inhomogeneities (Jeans, 1902) the Universe must become matter dominated (Guyot & Zeldovic, 1970). As later discovered, the baryon density is nearly an order of magnitude too low (Yang et al., 1984) for this, and since we clearly observe structure some additional form of dark matter must also exist in order for the Universe to be matter dominated.

There are three broad groups of dark matter candidates: hot dark matter, warm dark matter, and cold dark matter. Hot dark matter is relativistic and collisionless (e.g. Bond & Szalay, 1983), while warm dark matter is non-relativistic when the horizon scale is galaxy-sized (e.g. Pagels & Primack, 1982), and could be neutrinos or gravitinos.

Because hot dark matter's free-streaming damping mass is on the order of the size of galaxy clusters, then galaxy clusters would be the first structure to form in this top down model, and then they would break up into galaxies and then dwarf galaxies. For warm dark matter, galaxies would form first.

Cold dark matter (Blumenthal et al., 1984), on the other hand, is non-relativistic. It leads to a hierarchical formation scenario of the Universe where small halos form first, and later these collect into galaxies, and within them gas cools into stars. In only the most dense regions of the Universe the galaxies come together into galaxy clusters, as described by Press & Schechter (1974).

There is more evidence for this model, given that galaxies are older than clusters, and galaxies have been caught in the process of merging (e.g. Neuschaefer et al., 1997). Early candidates for cold dark matter included non-baryonic possibilities such as small black holes. Baryonic candidates included dark planets or brown dwarfs, but now dark matter is believed to be either mostly or entirely non-baryonic in composition (Sadoulet, 1999) after extensive microlensing searches. Today, a number of particles are still up for consideration, the most popular class being weakly interacting massive particles (WIMPs) like axions and photinos (Muñoz, 2004).

Since then the properties of cold dark matter, and the curvature and composition of the Universe as a whole has been measured to great precision. The Cosmic Microwave Background (CMB) is a residual black body radiation remaining from high temperatures early in the Universe's history, first hypothesized by Alpher et al. (1948) to explain the chemical abundances of elements. Discovered by Penzias & Wilson (1965) and simultaneously identified by Dicke et al. (1965), the CMB proved to be a powerful tool because important information about the Universe's structure lies encoded in the CMB anisotropies, as first detected with COBE (Smoot et al., 1992). The Wilkinson

Microwave Anisotropy Probe (WMAP3) (Spergel et al., 2007) has now been able to measure many of these cosmological parameters to high precision:

$$\Omega_m h^2 = 0.1277_{-0.0079}^{+0.0080} \quad (1.1)$$

$$\Omega_b h^2 = 0.02229 \pm 0.00073 \quad (1.2)$$

$$h = 0.732_{-0.032}^{+0.031} \quad (1.3)$$

$$n_s = 0.958 \pm 0.016 \quad (1.4)$$

$$\tau = 0.089 \pm 0.0030 \quad (1.5)$$

$$\sigma_8 = 0.761_{-0.048}^{+0.049} \quad (1.6)$$

Combining WMAP with the Supernova Legacy Survey (Astier et al., 2005) yields:

$$w = -0.967_{-0.072}^{+0.073} \quad (1.7)$$

while combining it with the HST Key Project (Freedman et al., 2001) constrains

$$\Omega_k = -0.014 \pm 0.017 \quad (1.8)$$

$$\Omega_\Lambda = 0.716 \pm 0.055 \quad (1.9)$$

## 1.2 The Missing Satellites Problem

There do remain outstanding issues with  $\Lambda$ CDM. While observations of dwarf halos imply cored centres, simulations have cuspy centres (Flores & Primack, 1994) and the central concentrations of N-body galaxies are too dense (Navarro & Steinmetz, 2000). Additionally, simulated galaxies reveal

more substructure in galaxies than what is actually observed (Moore et al., 1999; Klypin et al., 1999).

In a hierarchical Universe, substructure is expected to be present at a similar level at all scales of interest. In some of the earliest cosmological simulations that were able to resolve substructures, Moore et al. (1999) found that dark matter-only simulations of galaxies and galaxy clusters had the same number of substructures relative to the total mass of the system. A comparison of the simulations to observations showed that the simulated galaxy cluster matched the quantity of substructure in the nearby Virgo cluster, but that the simulated galaxy had significantly more substructure than the Local Group. Using constrained simulations of a system similar to the Local Group, Klypin et al. (1999) found far more substructure than what has been observed. This discrepancy between  $\Lambda$ CDM and observations is known as the “missing satellites problem”. Kravtsov (2010) provides a recent review of the progress made towards solving this problem.

Generally, there are two paths pursued to resolve the missing satellites problem. One is to alter the cosmological paradigm. Examples of this include self-interacting dark matter in which subhalos are destroyed through self-annihilation (Spergel & Steinhardt, 2000), warm dark matter (Dalcanton & Hogan, 2001), or altering the primordial power spectrum (Zentner & Bullock, 2003). The other path is to consider the effects of baryonic physics, such as stellar feedback (Dekel & Silk, 1986; Mac Low & Ferrara, 1999) or the ultra violet (UV) background ionisation (Efstathiou, 1992; Quinn et al., 1996; Bullock et al., 2000), which might cause many satellites to be composed of

dark matter only, or at least no stars, rendering them invisible to observations. Recent gravitational lensing studies using galaxies (Dalal & Kochanek, 2002) have discovered dark substructures, as also explored with simulations (Mao et al., 2004), though the total number of substructure is still up for debate. So if we accept the  $\Lambda$ CDM as it is, the next natural question is what physical mechanisms play the largest role in darkening small galactic halos and preventing star formation.

### 1.3 Solving the Missing Satellites Problem: Mechanisms for Baryon Removal

There are four primary mechanisms that can remove baryons, mostly gas, from subhalos:

- **UV ionisation:** hydrogen in the early universe is ionised by the ultra violet radiation, believed to be emitted by the first luminous objects in the reionisation epoch. This sets the background temperature of the intergalactic medium to be higher than that of the subhalos' own virial temperatures in all but the heaviest subhalos. Later on, the UV ionisation stems from sources in the host halo itself.
- **Ram pressure stripping:** as a satellite glides through the hot halo gas pressure becomes stronger than the gravitational force that binds gas to the subhalo itself, and is subsequently removed.

- **Stellar feedback:** stellar winds and supernovae inject enough energy into the interstellar medium (ISM) of the small subhalo that is strong enough to eject gas from the lower mass subhalos.
- **Tidal stripping:** when a subhalo nears its larger host galaxy the tidal forces become sufficient to remove material. Unlike the other three mechanisms mentioned above this is the only one that can remove collisionless matter, like dark matter and stars, as well as gas from a subhalo.

Previous efforts have been made at examining these mechanisms in detail. Many of these efforts have been analytical due to the large dynamic range necessary to properly simulate substructures. Dekel & Woo (2003) compared careful observations of many dwarfs with an analytical model based on the effect of supernova feedback and found that supernova feedback defines the line between low and high luminosity dwarf galaxies. Kravtsov et al. (2004) used high resolution, cosmological simulations to study the role of tidal stripping in the mass evolution of satellites. They concluded that the combined effect of tides and ionisation could produce a Milky Way-like satellite luminosity function. Read et al. (2006) considered both stellar-driven winds and ionisation in cosmological simulations and found that ionisation was critical to make their simulations agree with observed luminosity functions. Governato et al. (2007) found in another series of cosmological simulations that the UV background dramatically reduced the number of luminous subhalos, but that supernovae feedback was required to make the simulated luminosity functions the same as those observed.

More recent cosmological simulations by Okamoto et al. (2009) have varied the strength of a kinetic supernova wind feedback to determine exactly how much energy is required to produce the observed luminosity function. Klimontowski et al. (2010) saw how tidal stripping determines a subhalo's baryon content and final morphology. Wadepuhl & Springel (2010) introduced black holes into their simulations and found that the black holes are not massive enough in subhalos to have an effect on their luminosities. They did, however, find that wind-driven stellar feedback can reduce the number of high mass satellites, and cosmic rays can suppress the luminosity of low mass subhalos. Each of these models successfully fit the data by emphasizing one or two mechanisms.

One study has pointed out the importance of the combined effects of each mechanism. Mayer et al. (2006) simulated individual satellites falling into a static gravitational potential filled with hot, dense gas. In these simulations, tidal forces excite star formation and thus stellar feedback, as well as reshaping the gas distribution so that it can be more easily stripped due to ram pressure. Mayer et al. (2006) called this combination of processes “tidal stirring” and found that it can remove enough gas from dwarf irregulars to turn them into gas-poor dwarf spheroidals.

The mass a halo has had in the past, either at its birth or at the time of accretion into its host, certainly plays a role in its final baryon content. Only the more massive subhalos (Okamoto & Frenk, 2009; Guo et al., 2009; Macciò et al., 2009) retain stars, and mass-dependent star formation-suppression mechanisms could be key (Koposov et al., 2009). The subhalos around a semi-

analytic model of an N-body simulation of a Milky Way-like halo (Li et al., 2009), reveal luminous subhalos whose mass in dark matter spanned one order of magnitude, while the luminosity ranged over five orders of magnitude, matching observations. There were also many more dark matter-only subhalos present, whose mass spanned three orders of magnitude.

## 1.4 Dwarf Galaxies

Classically, the dwarf galaxies have been divided into three categories: dwarf ellipticals, dwarf spheroidals, and dwarf irregulars (Grebel, 1997) as pioneered by the Sandage & Binggeli (1984) catalogue for galaxies in the Virgo cluster. Dwarf ellipticals are a faint extension of the elliptical galaxy category, with distinct nuclei (Ferguson & Binggeli, 1994). Dwarf spheroidals, on the other hand, have no nuclei and less gas than dwarf ellipticals (Gallagher & Wyse, 1994). Dwarf irregulars are the low surface brightness cousins of giant irregular galaxies, sharing many global properties like irregular morphology and large HI fractions, and are more gas-rich compared to other dwarf galaxies (Hunter & Gallagher, 1985). All together, these dwarf galaxies are the most common objects in the Universe today (Marzke & da Costa, 1997). Mateo (1998) compiled a comprehensive compendium on the classic dwarf galaxies in the Local Group. At the time thirty-six galaxies were known in the Local Group, their absolute V-band magnitudes ranging from  $M_V \sim -18$  to  $-8.8$

In recent years on the vanguard of large surveys, including the Sloan Digital Sky Survey, a new category of dwarf galaxies has been unearthed: the ultra faint dwarfs (Willman et al., 2005; Belokurov et al., 2007; Koposov et al.,

2008), adding to the total sum of luminous substructure in the Local Group and lessening the severity of the missing satellites problem. However, it does not entirely solve it given that there are about a factor of 4 too few observed dwarf galaxies still (Simon & Geha, 2007), though they suggest that there are ultra faint dwarfs out there that may be even less massive than what has so far been observed. Currently, these large surveys do not cover the entire sky and there may still be ultra faint dwarf galaxies too faint for current instrumentation. Tollerud et al. (2009) have estimated that around 300 to 600 dwarf galaxies may in fact exist within the Milky Way’s virial radius alone, some of them dark. Fundamentally, some dwarf galaxies may be populated with stars and some not, and a leading question is what causes the difference between these dwarf galaxies.

## 1.5 Outline

The science presented in this thesis consists of four sections. Chapter 2 will go over the background of our simulations, namely the McMaster Unbiased Galaxy Simulations (MUGS) galaxies we use for our analysis; the Amiga Halo Finder (AHF) invoked to identify the subhalos of every galaxy; our method of merger tree construction to track subhalos through time; and a quantitative introduction to the properties of the fourteen host galaxies featured in this paper. Chapter 3 will present the luminosity functions of the subhalos for these fourteen host galaxies and compare them to data from the Milky Way. We also re-simulate one host galaxy, g5664, by varying the baryonic physics to see the effects of stellar feedback and the UV background had on g5664’s luminosity

function. Chapter 4 will be dedicated to a single host galaxy, g15784, where we deconstruct the mechanisms by which baryons are driven from its subhalos: UV ionisation, tidal stripping, ram pressure stripping and stellar feedback. We explicitly track the causes behind the departure of individual gas particles from their subhalo in order to paint a comprehensive picture showing the relative strength of each. Lastly, Chapter 5 will return to multiple host galaxies and examine the relationship subhalos' maximum masses have to how luminous they become at redshift zero. The entire thesis will be concluded and discussed in Chapter 6.



## Chapter 2

### Method

#### 2.1 MUGS: The McMaster Unbiased Galaxy Simulations

We analyze the subhalos of fourteen galaxies from the McMaster Unbiased Galaxy Simulations (MUGS), with total masses between  $\sim 5 \times 10^{11} M_{\odot}$  and  $\sim 2 \times 10^{12} M_{\odot}$ . The purpose of MUGS is to provide a sample of  $L^*$  simulated galaxies. A full description of MUGS can be found in Stinson et al. (2010), but we briefly summarize it here. MUGS was run using the SPH code GASOLINE (Wadsley et al., 2004). GASOLINE includes low temperature metal cooling (Shen et al., 2010) using CLOUDY (version 07.02, last described by Ferland et al. (1998)) and assuming ionisation equilibrium, star formation, physically-motivated stellar feedback, and a spacially uniform ultraviolet ionising background adopted from Haardt & Madau (in preparation; see Haardt & Madau, 1996), is used in order to calculate the metal cooling rates self-consistently. The initial dark matter, gas and star particle masses are  $1.1 \times 10^6 M_{\odot}$ ,  $2.2 \times 10^5 M_{\odot}$  and  $6.3 \times 10^4 M_{\odot}$  respectively. Outputs were at most 214 Myr apart, especially

at lower redshift, with irregular outputs at key times. Outputs were much closer together at high redshifts, typically 107 Myr apart.

First,  $256^3$  dark matter particles were evolved to redshift zero in the  $50 h^{-1}$  Mpc box with periodic boundary conditions and a WMAP3  $\Lambda$ CDM universe ( $H_0=73 \text{ km s}^{-1} \text{ Mpc}^{-1}$ ,  $\Omega_m=0.24$ ,  $\Omega_\Lambda=0.76$ ,  $\Omega_{baryon}=0.04$ , and  $\sigma_8=0.79$ ) (Spergel et al., 2007). A number of random galaxies were selected from those with mass greater than  $\sim 2 \times 10^{12} M_\odot$  that did not evolve near a massive structure in order to be unbiased towards: angular momentum, merger history, and distribution of less massive neighbors in order to reproduce the spread in galaxy properties seen in observations. The only bias might arise from random chance. Merger history is defined as the redshift at which a galaxy achieves half of its final mass, and angular momentum is given by the definition used in Bullock et al. (2001),  $\Lambda = J/\sqrt{\frac{5}{3}GM^3R}$ . It is hoped that our sample will reproduce the observed spread in galaxy properties.

For each randomly selected galaxy the zoom renormalization technique (Governato et al., 2004) was used as described here. This involved marking off a region of interest around the galaxy, determined by finding all particles within five virial radii of the galaxy at redshift zero and tracing them back to their positions in the initial conditions. This leads to a non-spherical region of interest in order to save computational resources. These selected galaxies are then re-run at higher resolution with baryonic physics and now equivalent to  $2048^3$  particles, while keeping their neighboring filaments and galaxies at low resolution.

The star formation and feedback recipes use the “blastwave model” described in detail in Stinson et al. (2006). In order to form stars, gas particles must be dense ( $n \geq 0.1 \text{cm}^{-3}$ ) and cool ( $T \leq 15,000 \text{K}$ ). Then a randomly-selected subset of particles that qualify for this form stars according to:

$$\frac{dM_{\star}}{dt} = c^{\star} \frac{M_{gas}}{t_{dyn}} \quad (2.1)$$

where  $M_{\star}$  is mass of stars created,  $c^{\star}$  is a constant star formation efficiency factor,  $M_{gas}$  is the mass of gas creating the star,  $dt$  is how often star formation is calculated (1 Myr in all the MUGS simulations described in here) and  $t_{dyn}$  is the gas dynamical time. The constant parameter,  $c^{\star}$ , is tuned to 0.05 so that the simulated Isolated Model Milky Way used in Stinson et al. (2006) matches the Kennicutt (1998) Schmidt Law, and then  $c^{\star}$  is left fixed for all subsequent applications of the code.

Due to our resolution, having each star particle being about  $6.3 \times 10^4 M_{\odot}$ , the star particles in fact represent groups of stars. Each star particle is partitioned into mass bins given by the Kroupa et al. (1993) initial mass function and later assigned lifetimes according to Raiteri et al. (1996). Stars over  $8.0 M_{\odot}$  explode as supernovae after they expire, releasing energy in quantized packets as given by the Stinson et al. (2006) model as used in MUGS.

## 2.2 Group Finding: Amiga Halo Finder

In order to identify the host galaxy and its subhalos, we used the Amiga Halo Finder (AHF) (Knollmann & Knebe, 2009). AHF is based on the spherical overdensity method for finding halos. It is able to identify density peaks

using an adaptive mesh algorithm. Once the density peaks are identified, AHF cuts out halos (and subhalos) using isodensity contours. Particles belonging to subhalos are distinguished from those of the background halo using a simple unbinding procedure to determine whether the particles are gravitationally bound to the subhalo.

We base our analysis on a minimum group size of 50 particles, which is  $2.2 \times 10^7 M_{\odot}$  when the group only contains dark matter but could be less massive if it also contains gas and star particles. Our analysis is restricted to those satellites identified by AHF as lying inside the virial radius ( $r_{vir}$ ) of the halo. Because of this constraint, we expect the satellites we are analyzing to be similar to dwarf spheroidal (dSph) galaxies, a population that dominates the satellite population of the Milky Way within  $r_{vir}$ . Dwarf spheroidals contain little gas (e.g. Fig 3 in Grebel et al., 2003), but generally continued forming stars until recently (Skillman, 2007).

## 2.3 Merger Trees

We traced the histories of each subhalo in the galaxy. First, we identified groups at every output with AHF and then traced the particles present in the halos at  $z = 0$  back through the simulation including any gas out of which stars formed. For the sake of clarity, let us call the subhalo of interest ‘Alpha’. At each output, we note every group that contains Alpha’s particles. The group that had the largest number of Alpha’s particles is set as Alpha’s progenitor at that output. In this way, we trace the properties of each subhalo through time, including mass, distance from the host galaxy, and temperature.

Because this method only depends on the number of particles, a subhalo can jump in position space between outputs, switching between subhalos with different groups of particles. Such behavior was only observed in three of the highest mass subhalos in g15784, which will take most of this analysis in Chapter 4. This does not affect our results because the jumps only occurred at high redshifts and between subhalos of comparable mass and position that were soon to merge. The pivotal point of analysis in each subhalo history is its maximum mass, as will be show in Chapter 4, and it occurs well after any jumping behavior we see. Also, we will only look at the *last* time that a particle leaves its subhalo in order to prevent a single gas particle from being double-counted. Therefore, any event of gas being “lost” due to subhalo jumping will automatically be removed from the analysis.

## 2.4 The Fourteen MUGS Galaxies

To date, fourteen MUGS galaxies have finished running at high resolution with baryonic physics. Their masses, virial radii and the number of gas, star, and dark particles at redshift zero is given in Table 2.4, representing the diversity in sizes MUGS has to offer. The total mass of satellites in the system, the number of satellites and the number of luminous ones found by AMIGA at redshift zero are also included.

The percentage of total mass contained in substructure to the host galaxy mass was probed by Dalal & Kochanek (2002) using gravitational lensing, and they found it to be between 0.6% and 7%. Most of our systems fall between 2% to 6%, though there were a number of exceptions that had an excess of

Galaxy	Mass ( $10^{11}M_{\odot}$ )	$R_{vir}$ (kpc)	$N_{gas}$ ( $10^5$ )	$N_{star}$ ( $10^6$ )	$N_{dark}$ ( $10^5$ )	$Mass_{sat}$ ( $10^{10}M_{\odot}$ )	$N_{sat}$	$N_{lume}$
g7124	4.5	144	1.1	1.1	3.4	6.6	33	9
g5664	5.2	152	1.8	1.1	4.0	2.3	40	7
g8893	6.2	160	1.9	1.4	4.6	2.3	60	13
g1536	7.0	167	2.4	1.4	5.3	1.1	49	7
g21647	7.7	172	2.7	1.6	5.8	11	61	11
g24334	7.7	193	3.3	2.4	8.2	14	107	25
g22795	8.7	180	2.7	1.5	6.6	2.6	87	13
g22437	8.8	180	3.5	1.6	6.6	4.2	69	6
g422	9.5	183	3.2	1.9	6.9	24	98	15
g3021	11	192	3.4	2.4	7.9	6.7	96	19
g28547	11	193	3.4	2.5	8.1	20	92	19
g25271	13	206	4.0	2.4	10	2.8	107	17
g15784	14	212	4.8	2.6	11	8.5	107	23
g15807	21	242	7.8	4.0	17	8.4	147	31

Table 2.1: The attributes of every MUGS galaxy run to date, arranged in ascending order of mass. The virial radius as found by AHF, number of gas, star and dark particles are also given with the total mass of satellites found by AHF at redshift zero, the number of satellites and the subset of those that are luminous.

substructure above the lensing results: g21647 at 14%, g7124 at 15%, g24334 and g28547 at 18%, and g422 at 25%.

## Chapter 3

# Simulated Luminosity Functions

The first type of analysis we undertook was to compare the satellite luminosity functions of fourteen of the MUGS galaxies to observations of the Milky Way, finding that those galaxies close to the Milky Way in mass match its function closely. We also re-simulated a smaller galaxy, g5664, with and without the UV background and stellar feedback to compare the effects the presence these two mechanisms have on the subhalo population as a whole.

### 3.1 Fourteen Systems of Satellites

AHF found substructure in all fourteen of the MUGS galaxies, the numbers given in Table 2.4. Heavier galaxies tend to have on order a hundred satellites, while lighter galaxies might have thirty.

In order to determine the luminosity of each subhalo, we used the fact that within MUGS each star particle represents a groups of stars, partitioned into mass bins based on the initial mass function given by Kroupa et al. (1993). We extracted the brightness of the stars on the luminosity grid provided by CMD 2.1 (Leitherer et al., 1999; Marigo et al., 2008). Using the grid, we

performed a bilinear interpolation over the stellar ages and metallicities of each star particle and then summed the luminosities of all the star particles in each satellite to derive a stellar magnitude for the satellites. We neglect the effects of dust extinction since dwarf galaxies are low metallicity and rarely appear dust obscured (Mateo, 1998; Lisenfeld & Ferrara, 1998).

Figure 3.1 shows the cumulative luminosity function of the subhalo populations of the fourteen host galaxies, ordered by mass, in the V-band at  $z = 0$ . This is alongside data compiled by Tollerud et al. (2008) that includes both the classical satellites and the new ultra-faint dwarf galaxies of the Milky Way. It is believed that the set of ultra-faint dwarfs as observed is incomplete for now because of their faint luminosities and that the Sloan Digital Sky Survey does not cover the entire sky. We also provide a theoretical function from Koposov et al. (2008) given by  $\frac{dN}{dM_v} = 10 \times 10^{0.1(M_v+5)}$  that would represent a theoretical complete set of subhalos. They computed their function by correction for selection effect, and taking into account the probability a subhalo is detected as function of its distance to the Milky Way and its luminosity. The shape of this power law is not to be considered a predictor, but the normalization is. The resolution of our simulations is not high enough in order to say anything conclusive about the new classes of ultra faint dwarfs, however.

Recent measurements of the Milky Way put its mass at about  $1.0$  to  $1.5 \times 10^{12} M_\odot$  (Klypin et al., 2002; Dehnen et al., 2006). Most of our MUGS galaxies whose masses have about 77% to 90% of the Milky Way's mass (g21647, g22795, g422) and those whose masses approximately match it (g30211, g28547, g25271) have very similar culminative luminosity functions to the Tollerud

et al. (2008) incomplete function for their brightness limit. Tollerud et al. (2008) always goes dimmer due to the resolution of our simulations. The galaxies that are much lighter than the Milky Way's mass, ranging from  $\sim 70\%$  to  $45\%$  of its mass (g7124, g5664, g8893, g1536) have a much smaller cumulative number in substructure. The heavier satellites on the other hand that have around  $140\%$  and  $210\%$  of the Milky Way's mass respectively (g15784, g15807) have more luminous satellites than observed, and start to approach the Koposov et al. (2008) complete function. There are some surprises. While the masses of g24334 and g22437 are in the range of  $77\%$  and  $88\%$  of the Milky Way's, g22437 has much less substructure than the Milky Way, while g24334 nears the Koposov et al. (2008) theoretical function. The importance of having a sample of galaxies is exhibited in the variance in luminosity functions across galaxies of similar masses.

g22795 and g8893 follow the trend of the Tollerud et al. (2008) observed curve closely, while the other galaxies display an excess in high luminosity satellites compared to the Milky Way. This elbow in the high luminosity region is something that needs to be examined more as observations become powerful enough to probe the substructure in galaxies beyond the Local Group. There is the possibility that the Milky Way is an anomaly in producing too few luminous satellites. Conversely the Milky Way is a typical galaxy when it comes to luminosity functions, and the fact that almost all the MUGS galaxies display an excess might be because the star formation recipe produces too many stars.

Figure 3.2 shows the baryonic mass of the subhalo population of each galaxy as a function of total mass at  $z = 0$ . The points along the x-axis have zero

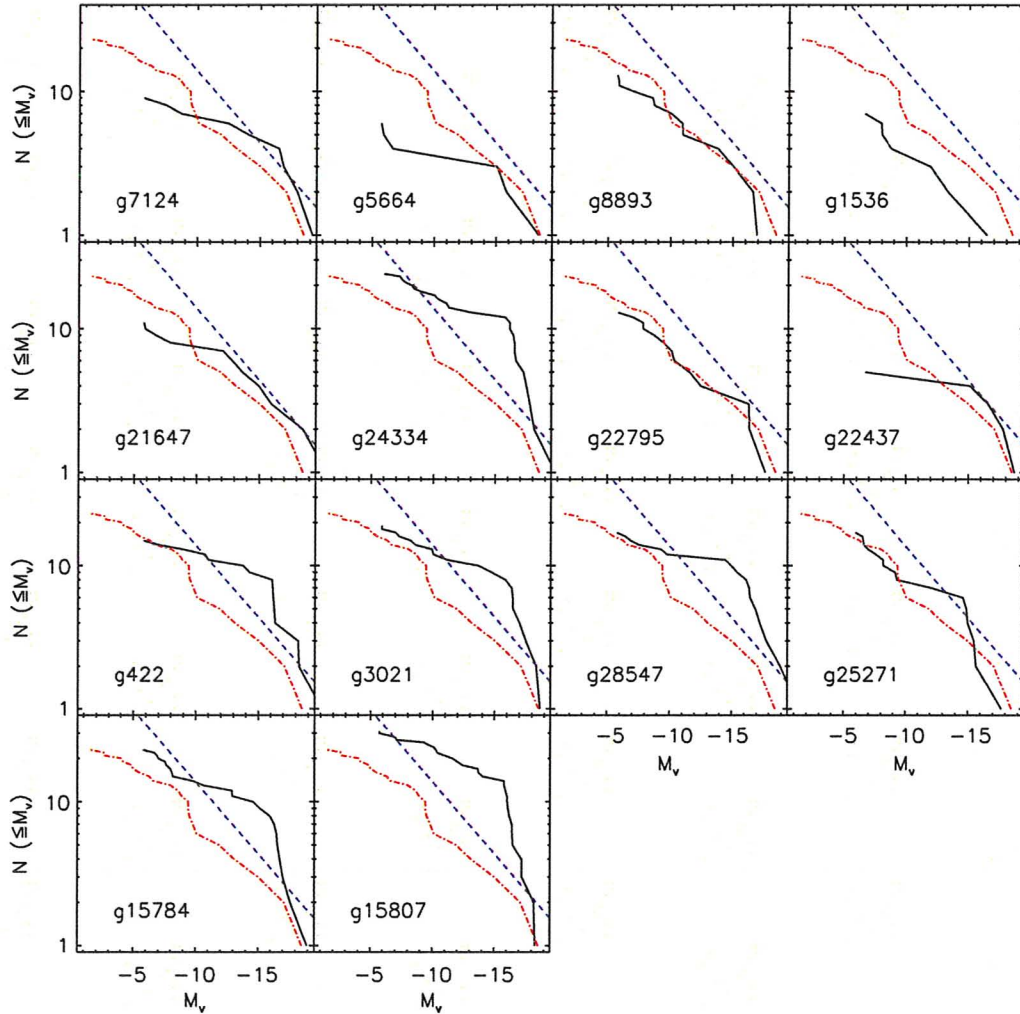


Figure 3.1: The cumulative V-band luminosity functions of the subhalo populations of the host galaxies at  $z = 0$ , in solid black, ordered by mass. Observational data of the Milky Way is gathered by Tollerud et al. (2008) in dashed-dotted red, and the theoretical function in dashed blue is from Koposov et al. (2009) as if the observations were complete. The ultra faint dwarfs as observed go much fainter than the resolution limit of our simulation. Lighter galaxies fall below both functions, as expected, while galaxies whose masses approach the Milky Way's tend to match the observations more closely.

baryon mass. With the exception of g22795, the high mass satellites follow a linear relationship as a function of the baryon mass, while this breaks down for lower mass satellites. The dashed line is the cosmic baryon fraction. The subhalos that exceed the cosmic baryon fraction generally follow a linear trend, while those below drop off. This falloff is similar to the observed trend found by McGaugh & Wolf (2010). g1536 and g5664 do not have enough luminous satellites for any trends to be noticeable. The most significant thing in these plots is that the zero baryon mass satellites (i.e. the dark satellites) and the luminous satellites overlap in their total mass, meaning that in any given galaxy, the luminous satellites are not all the most massive.

Figure 3.3 gives a detailed breakdown of this situation for one galaxy, g15784, where the satellites are divided into bins based on mass-to-light ratio. Luminous subhalos above  $5 \times 10^8 M_{\odot}$  having a mass-to-light ratios of at least 10 are fit with a powerlaw of index 0.9. Below this mass, subhalos contain systematically fewer baryons than the continuation of this power law indicates. Additionally, below  $2 \times 10^9 M_{\odot}$  there are many subhalos that contain no baryon particles at all and are thus dark. Of the 23 subhalos that have baryons, only 10 contain gas. This fraction might seem low if compared to high gas fractions found in isolated dwarf irregular galaxies (Geha et al., 2006), but the subhalos considered here are all within  $r_{vir}$  and are more appropriately compared with the dwarf spheroidals presented in Grebel et al. (2003), which are gas-poor.

We must stress that when we say a subhalo “has no baryons”, we mean in the sense of the simulation resolution there are no baryon particles. Of course actual dark subhalos will always have at least some trace quantities of gas.

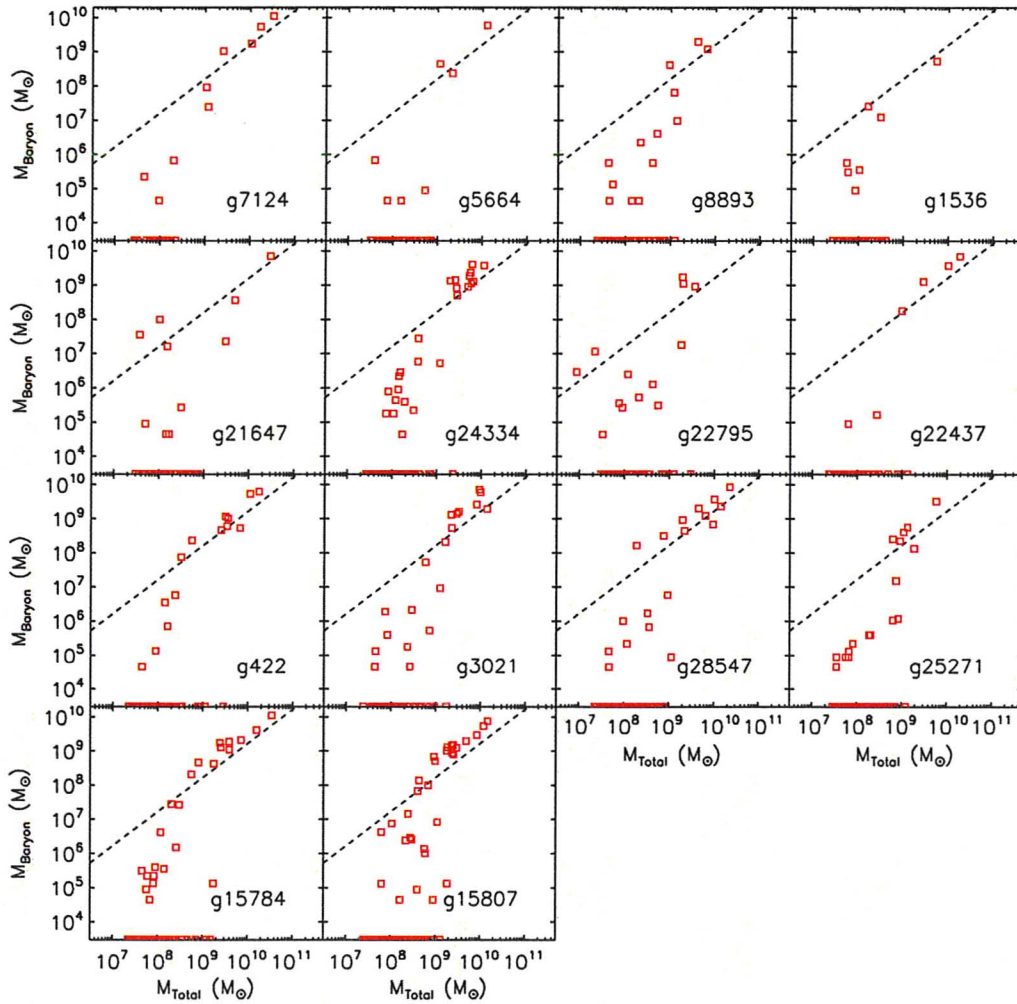


Figure 3.2: Baryon mass versus total mass for our subhalo population in all galaxies. The subhalos whose baryon mass falls on the x-axis in fact have no baryon particles and were moved there for the sake of displaying them on a log scale. Most striking here is that for every galaxy the luminous subhalos and dark subhalos overlap in total mass. The dashed line represents the cosmic baryon fraction. The subhalos that exceed the cosmic baryon fraction generally follow a linear trend, while those below drop off.

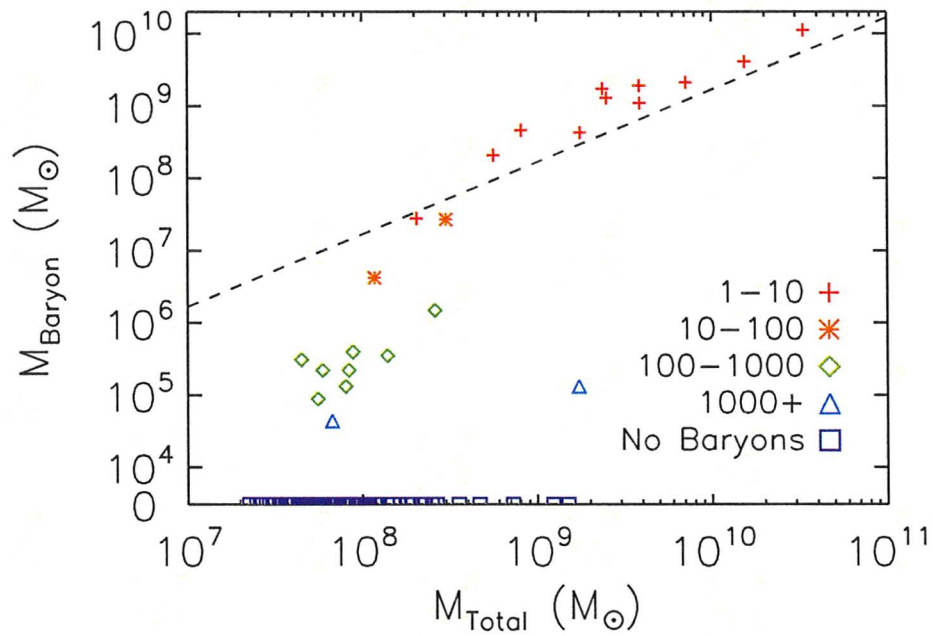


Figure 3.3: Baryon mass versus total mass for the subhalo population of g15784. The legend shows the symbols corresponding to mass-to-light ratio (total mass divided by baryonic mass), and the dashed line is the data for the subset of subhalos with  $M_{\text{total}} \geq 5 \times 10^8 M_{\odot}$  that have a mass-to-light ratio of at least 10 fit to a power law, given by  $M_{\text{baryon}} \propto M_{\text{total}}^{0.9}$ . The lower bound of the mass-to-light ratio is inclusive.

Figure 3.4 shows the cumulative mass function at  $z = 0$  for all the satellites in the galaxies as well as the subset that formed stars. The total satellite mass function for the heavier galaxies is similar to the collisionless, dark matter-only simulations of the Moore et al. (1999)  $2 \times 10^{12} M_{\odot}$  galaxy with the same order of magnitude of substructure, while the mass function of luminous satellites is closer to what is observed. In every galaxy there is about an order of magnitude more subhalos in total than those that contain baryons. How these dark subhalos lost their gas and their stars, if they ever had any, is the key to understanding the missing satellites problem. We investigate gas removal mechanisms, the reason some subhalos are luminous and some are dark by looking at one galaxy, g15784, in more detail in Chapter 4.

## 3.2 Effects of Stellar Feedback and Ultraviolet Background: g5664

One test to delve deeper into how the cumulative mass function can be consistent with dark matter-only simulations while the luminosity function is consistent with observations is to re-simulate a galaxy with and without the UV ionising and stellar feedback. We re-simulated a second, smaller host galaxy, g5664, with a mass of  $5.2 \times 10^{11} M_{\odot}$ , three times with different baryonic physics:

- (a) with the standard MUGS simulation including UV and stellar feedback,
- (b) with UV but no stellar feedback, and
- (c) with neither UV nor stellar feedback.

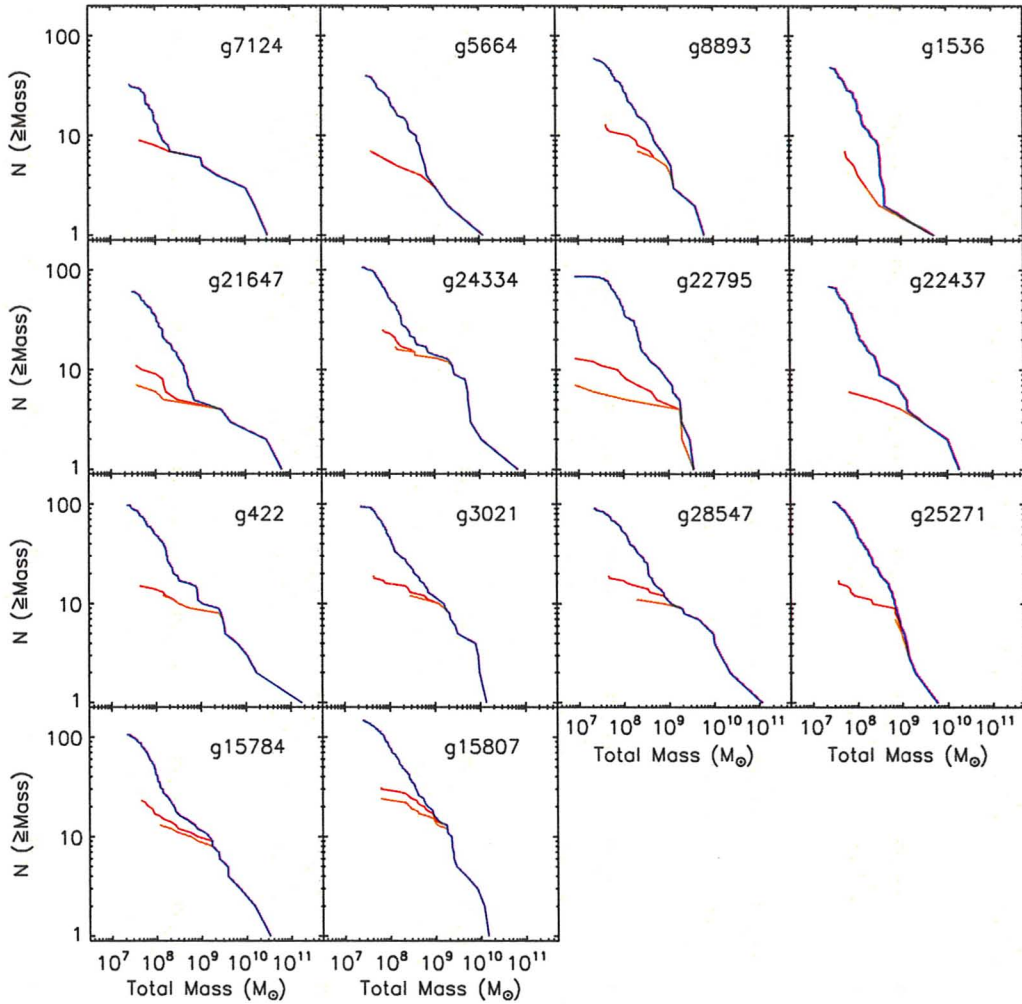


Figure 3.4: The cumulative mass function of the subhalo population of each galaxy at  $z = 0$ , divided into all subhalos in blue, those with baryons in red, and those with V-band magnitude (bright) greater than 10 in orange. For galaxies with their mass close to the Milky Way's the cumulative number for all subhalos are around a hundred, whereas only those subhalos with baryons have about an order of magnitude lower in cumulative number.

This galaxy is the second lightest of all MUGS galaxies and thus was faster to run, which is why it was chosen for the parameter comparison.

Figure 3.5 shows the cumulative luminosity function for the three simulations at  $z = 0$ . Nearly every satellite in the simulation run without feedback and UV (c) contains stars. Conversely, many fewer satellites contain stars in the simulation that includes both (a). Clearly the UV ionisation plays a large role in stopping stars from forming in many halos. The addition of stellar feedback has little effect on halos brighter than  $M_V \sim -15$ , but fainter halos are more vulnerable to having stellar feedback pushing out their gas early on and stopping further star formation. The  $M_V \sim -15$  threshold is similar to the flattening seen in Figure 3.1 for both the simulated and the observed Local Group mass function. Strangely enough, g5664 seems to have a dearth of satellites between  $-8 < M_V < -15$ , which may indicate a need for stronger feedback in simulations.

In addition Figure 3.6 shows that the total cumulative mass function is reduced by both the feedback and ultraviolet background. Clearly, both mechanisms working together are important and affect the subhalo population as a whole.

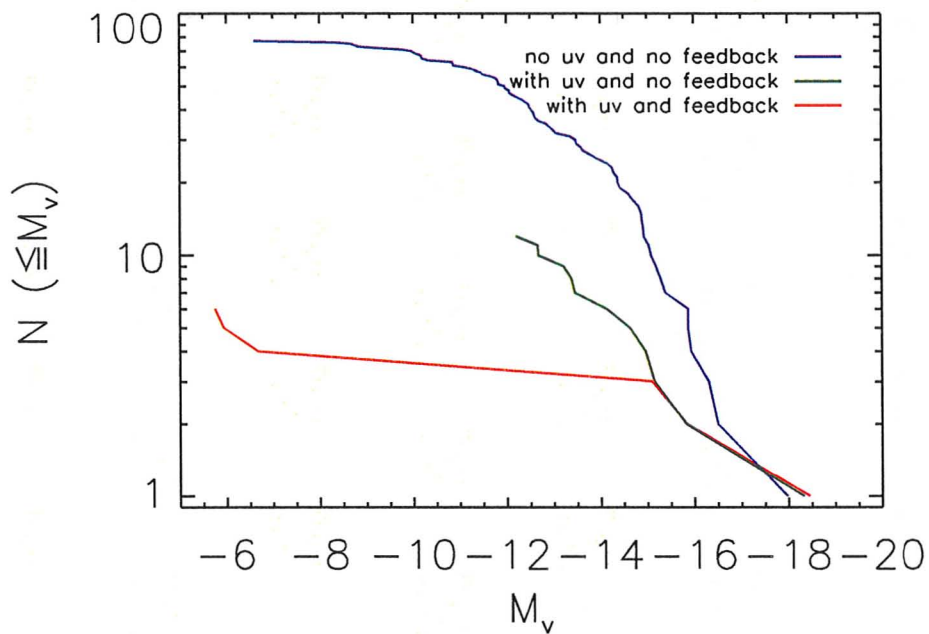


Figure 3.5: Cumulative luminosity function for g5664, comparing runs with three different conditions on the baryonic physics. The run with UV background and stellar feedback is in red (a). The run with UV background, but no feedback is in green (b). The run with neither UV background nor stellar feedback is in blue (c). Both feedback and UV background, when turned on, reduce the total number of luminous subhalos.

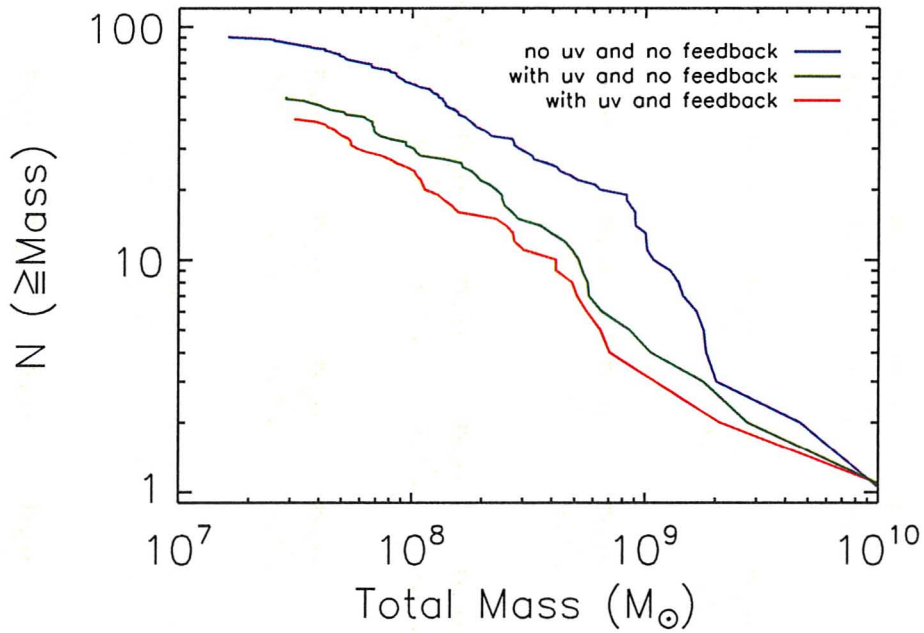


Figure 3.6: Cumulative mass function for g5664, comparing runs with three different conditions on the baryonic physics. The run with UV background and stellar feedback is in red (a). The run with UV background, but no feedback is in green (b). The run with neither UV background nor stellar feedback is in blue (c). Both feedback and UV background, when turned on, reduce the total number of subhalos.

## Chapter 4

# Gas Loss Mechanisms Through Satellite Histories: g15784 in Depth

The previous section showed that both stellar and UV feedback play a significant role in the evolution of satellite galaxies. In order to gain an overall picture of how stellar and UV feedback work with ram pressure and tidal stripping, we will focus on g15784 and look at the detailed, particle-by-particle mass loss history of its subhalos. g15784 has a mass of  $1.43 \times 10^{12} M_{\odot}$ , a disk of  $3.27 \times 10^{10} M_{\odot}$  and a bulge of  $5.49 \times 10^{10} M_{\odot}$ . This galaxy was chosen for its stability and the large number of satellites it has to provide a good population sample for analysis.

We traced the evolution of 85 of the 107 subhalos identified by AHF in g15784. We were unable to do a detailed trace of every halo for two reasons. 17 low mass subhalos did not maintain 50 member particles throughout the simulation. 5 subhalos were coincident with another halo during one output, and thus appeared to gain a large amount of mass. Later on this section, the analysis will focus on cumulative baryon loss and the subhalos' maximum

mass, and so these sudden spikes in mass would fudge any results if such subhalos were to be included in the analysis.

10 of the 85 subhalos we analyzed contained both gas and stars at  $z = 0$ , with total masses ranging from  $5.6 \times 10^8 M_\odot$  to  $3.3 \times 10^{10} M_\odot$ . Of the subhalos that did not have gas at  $z = 0$ , 17 formed stars at some point but only 13 of these retained them until  $z = 0$ . This leaves a total of 23 luminous subhalos at redshift zero.

Figure 4.1 to 4.3 show examples of the time evolution of nine subhalos' mass and distance to the host, labelled sh1 to sh9. Figure 4.1 shows three massive subhalos (sh1 to sh3) that retain both gas and stars at redshift zero. Figure 4.2 shows three medium to low mass subhalos (sh4 to sh6) that form stars at some point in their lives, but only sh4 and sh5 hold on to them at redshift zero, being luminous, while sh6 is a dark satellite. Figure 4.3 shows three medium to low mass subhalos (sh7 to sh9) that never form stars and lose their gas quickly, all ending up as dark satellites at redshift zero. The masses of all nine subhalos are given in Table 4.1, along with the maximum mass the subhalos achieve over its lifetime. This maximum mass will become important in §4.5.

Gas, and to a lesser extent dark matter, is significantly affected by close passages to the host, while stars once formed tend to sit undisrupted within the subhalo, at least for the higher mass subhalos sh1 to sh3. The lower mass subhalos, sh4 to sh6, are affected more strongly, having their stars tidally stripped across several close passages.

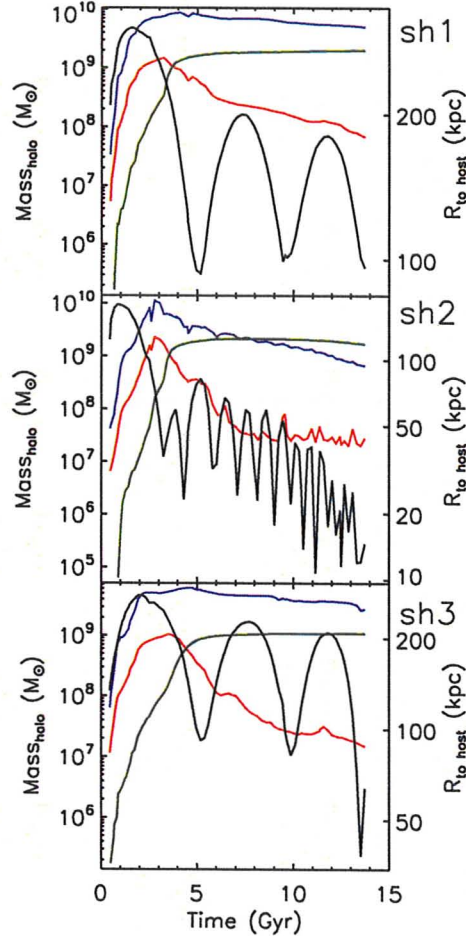


Figure 4.1: The time evolution of the distance to the host and the mass of three massive subhalos in g15784. From top to bottom they are labelled as sh1, sh2, and sh3. The black line corresponds to the distance to the host on the right-hand axis on each plot. The coloured lines correspond to the masses on the left-hand axis: dark matter (blue), gas (red) and stars (green). All three subhalos are massive enough the retain both gas and stars at redshift zero.

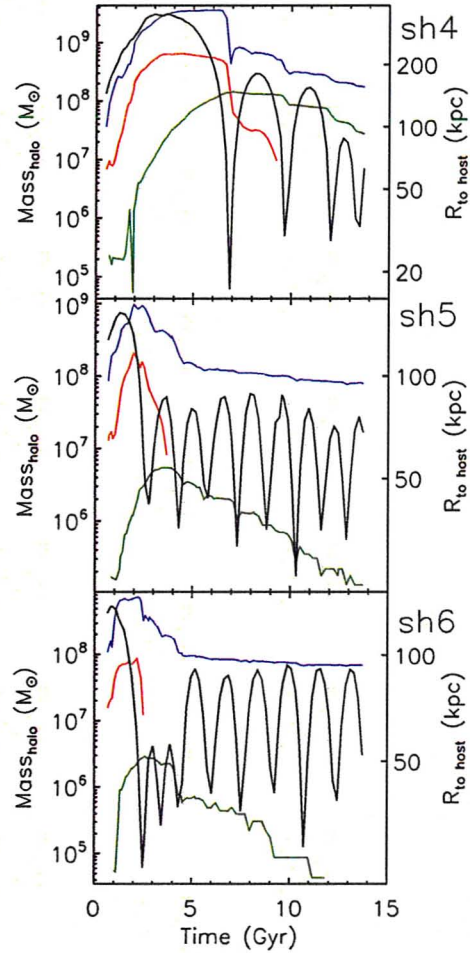


Figure 4.2: The time evolution of the distance to the host and the mass of three medium to low mass subhalos in g15784. From top to bottom they are labelled as sh4, sh5, and sh6. The black line corresponds to the distance to the host on the right-hand axis on each plot. The coloured lines correspond to the masses on the left-hand axis: dark matter (blue), gas (red) and stars (green). All three subhalos form stars at some point in their lives, but only sh4 and sh5 retain them to redshift zero. sh6 ultimately ends up as a dark satellite.

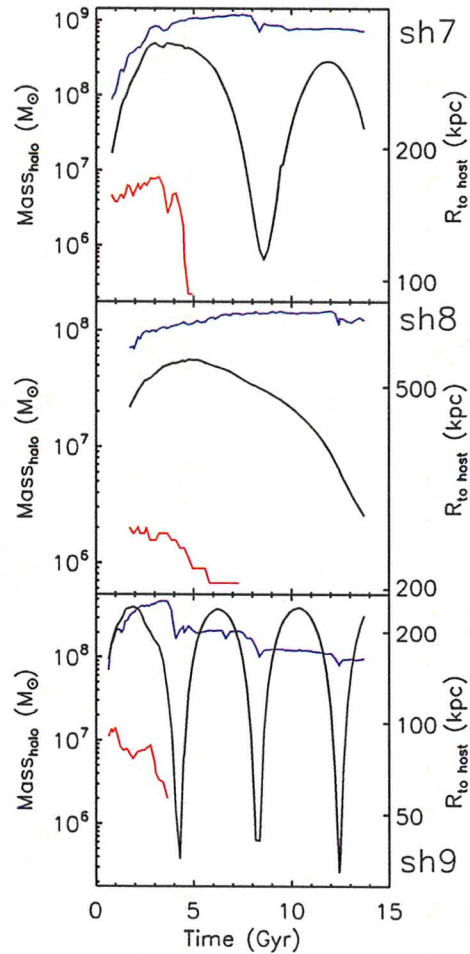


Figure 4.3: The time evolution of the distance to the host and the mass of three medium to low mass subhalos in g15784. From top to bottom they are labelled as sh7, sh8, and sh9. The black line corresponds to the distance to the host on the right-hand axis on each plot. The coloured lines correspond to the masses on the left-hand axis: dark matter (blue), gas (red) and stars (green). All three subhalos lose their gas quickly and never form any stars, ending up as dark satellites.

Subhalo	Final Mass ( $10^9 M_{\odot}$ )	Maximum Mass ( $10^9 M_{\odot}$ )
sh1	7.1	11
sh2	2.3	14
sh3	3.9	7.4
sh4	0.20	4.2
sh5	0.080	1.2
sh6	0.069	8.3
sh7	0.72	1.2
sh8	0.12	0.15
sh9	0.095	0.48

Table 4.1: The mass at redshift zero and the maximum mass ever achieved over time for the nine subhalos that we follow in Figures 4.1 to 4.3.

The quantity of gas lost is also mediated by the proximity of the subhalo to the host, and the most significant drops happen at the pericentres. However, proximity to the host does not tell the full story. The subhalo that stays the closest to the host is sh2, with more than ten close passages and a pericentre between 10 and 20 kpc. It is however amongst the most massive and luminous subhalos, though by redshift zero it has lost much of its gas. Conversely, dark sh8 is the most distant subhalo, who was at one point 500 kpc away and is only at redshift zero just beginning to fall into its host, still at a distance of 300 kpc. sh7 is also distant. The fact that they are so far from the host galaxy also explains why they do not accumulate much gas to begin with, because they begin in regions of low gas-density.

We can also rank these subhalos according to their final mass. sh1 to sh3 are the three most massive and also the three most luminous shown here. However, the dark satellite sh7 is more massive than either the luminous sh4 or sh5, and dark sh8 and sh9 are more massive than luminous sh5. sh6, though

ultimately dark, did manage to have enough gas at some point to form stars, but it is also the lightest of the nine subhalos featured. There are more factors at work than a subhalo mass at  $z = 0$  and its proximity to the host galaxy that decide if it is luminous at  $z = 0$ .

Every one of the 85 subhalos with comprehensive histories managed to have gas at some point in its recorded history, whether or not there remains any gas, or baryons at all, at  $z = 0$ . Without fail, each subhalo loses gas on a close passage to the host galaxy. Often all gas is lost on the first encounter, while in other cases it can take two to five close passages before the gas is finally stripped.

If these subhalos manage to form stars before the first passage by the host, then the stars tend to remain safe deep within the potential well of the subhalo, unless the subhalo is not so massive and some stars get tidally stripped. Otherwise, if stars are not formed before this first passage then the subhalo will never form stars and will become a dark satellite.

## 4.1 Ultraviolet Background

Early speculations on the existence of the intergalactic medium (IGM) were purely theoretical in motivation, its source either baryons leftover from galaxy formation or baryons stripped from galaxies (Ikeuchi & Ostriker, 1986) until observations of X-ray emissions could confirm its existence (Forman & Jones, 1982; Mushotzky, 1983). Later studies of the quasar spectra uncovered photoionisation of this IGM (e.g. Webb et al., 1992), known as the ultraviolet (UV) background radiation to redshifts of at least 5.8 (e.g. Fan et al., 2000).

The Gunn-Peterson Trough (Gunn & Peterson, 1965) was predicted to appear in the spectra of quasars from neutral hydrogen in the IGM before reionisation. Becker et al. (2001) discovered this in a  $z \sim 6.28$  quasar, while the lack of the Gunn-Peterson Trough in a  $z \sim 5.99$  quasar sets the reionisation epoch to now be about  $z \sim 6$ . Rauch (1998) reviews the observations. There are several phenomena that are candidates for generating the UV background (Henry, 1991), the most prominent being star-forming galaxies and quasars (e.g. Haardt & Madau, 1996; Schirber & Bullock, 2003; Dall’Aglio et al., 2009).

Through analytical calculations Rees (1986) suggested that this UV background could prevent low-mass objects from collapsing, and Efstathiou (1992) found that it could suppress star formation in dwarf galaxies due to lengthening the cooling time of gas. Later simulations (Quinn et al., 1996; Thoul & Weinberg, 1996) showed that this is indeed the case, and that the UV background plays an important role in creating the observed luminosity function. With the advent of the missing satellites problem the UV background has also been used as part of the solution in creating the dark satellites (e.g. Bullock et al., 2000)

We confine our analysis of the evolution of subhalos to the time after  $z = 10.8$ , when a few groups get larger than the minimum AMIGA particle limit and have virialized. One of the earliest mechanisms that removes gas from subhalos is the ionising UV background radiation that is emitted from the first luminous objects. This radiation makes its first impact at  $z = 9.9$  in our simulations. However, most groups do not form until after the the UV

background has turned on, and so we need an alternative means of tracking the subhalos before *and* after  $z = 9.9$  without using the group finder.

To enable our analysis of the effects of UV radiation, we match every dark matter particle within the high resolution virial radius with a “twin” gas particle at the initial conditions. In our halo-by-halo analysis, we find the twin for every dark matter particle in a subhalo at the output of the subhalo’s maximum mass. We then follow the evolution of the gas twins, from the first output to the last. We refer to the ensemble of these twin gas particles for a halo as the background gas.

What we find is that unless the dark subhalo forms before reionisation, most of the background gas to the subhalo never joins the group at all. However, a few of the dark subhalos that formed after reionisation accreted other gas and formed stars. Thus, the gas twin analysis might be insufficient, so we developed an alternate means of determining the effect of UV radiation involving each halo’s virial temperature ( $T_{vir}$ ).

In order for a gas particle to have enough energy to overcome the potential of the subhalo and escape, its temperature must be at least:

$$T_{vir} = \frac{2G\mu m_p M_{subhalo}}{3kR_{subhalo}} \quad (4.1)$$

where  $G$  is the gravitational constant,  $\mu$  is the mean molecular weight, which here we take to be 0.6 for fully-ionised primordial gas with three hydrogen atoms to one helium mass-wise,  $m_p$  is the proton mass,  $k$  is Boltzmann’s constant, and  $M_{subhalo}$  and  $R_{subhalo}$  are the mass and radius of the subhalo respectively, where the subhalo is approximated by a self-gravitating sphere. We define this as the virial, or escape, temperature of the subhalo.

Figure 4.4 shows a comparison of  $T_{vir}$  with the mean background gas temperature, and the temperature of the subhalo gas identified as belonging to sample subhalos. An analysis of the same comparison for all the subhalos shows that, with one exception, every subhalo that at some point has a background gas temperature lower than  $T_{vir}$  ( $T_{vir}/T_{background} > 1$ ) captures enough gas to form stars. Figure 4.4 shows the evolution of the background temperature and the virial temperature of two subhalos over time. In Figure 4.4, the lower mass subhalos at  $z = 0$  formed stars, while the second subhalo failed to form stars since its  $T_{vir}$  was always lower than that of its background gas. Thus, the “twin” particle analysis appears to be robust.

Figure 4.5 shows a summary comparison of  $T_{vir}$  with halo background temperatures. Specifically, we compare the maximum ratio over time of  $T_{vir}$  to background gas temperature as a function of the baryon fraction at each start for a subhalo and  $z = 0$ . The subhalos that obtain  $T_{vir}/T_{background} > 1$  at some point in their lives all start near the cosmic baryon fraction. With one exception, the subhalos that hold on to baryons at  $z = 0$  are a subset of these. That exceptional satellite started out near to the host, was able to gather much gas quickly to form enough stars to remain luminous during its subsequent several close passages to the host, while it lost all gas on its second passage.

Quantifying just how much gas a subhalo loses due to the UV background induces some level of subjectivity. Instead of merely counting gas that was in the subhalo, it involves determining how much gas was never in the subhalo but ought to have been. Furthermore, this is complicated by the fact that AHF

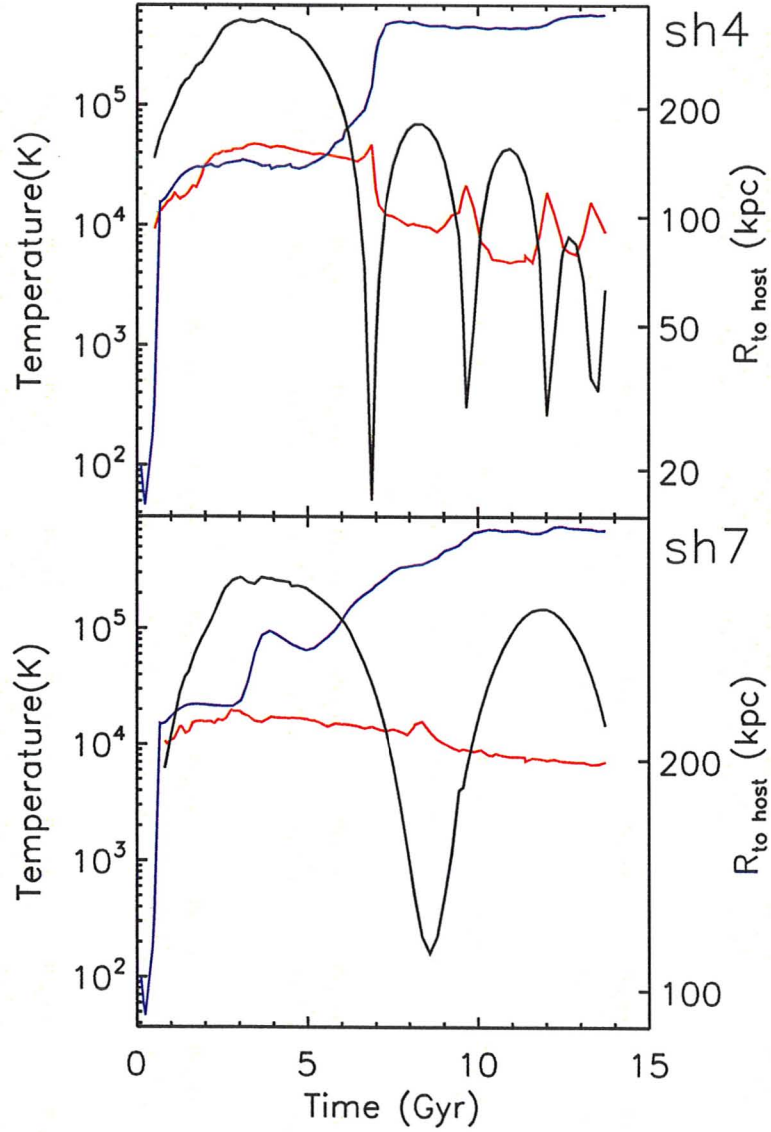


Figure 4.4: Temperature of background gas (blue) and the subhalo  $T_{vir}$  (red) for subhalos sh4 (Figure 4.2) and sh7 (Figure 4.3) in g15784. Temperature corresponds to the left axis, and the subhalo orbits (black) to the right. Even though sh7 is more massive at  $z = 0$ , it is unable to retain as much gas as sh4 due to the fact that its  $T_{vir}$  is consistently lower than the temperature of its background gas.

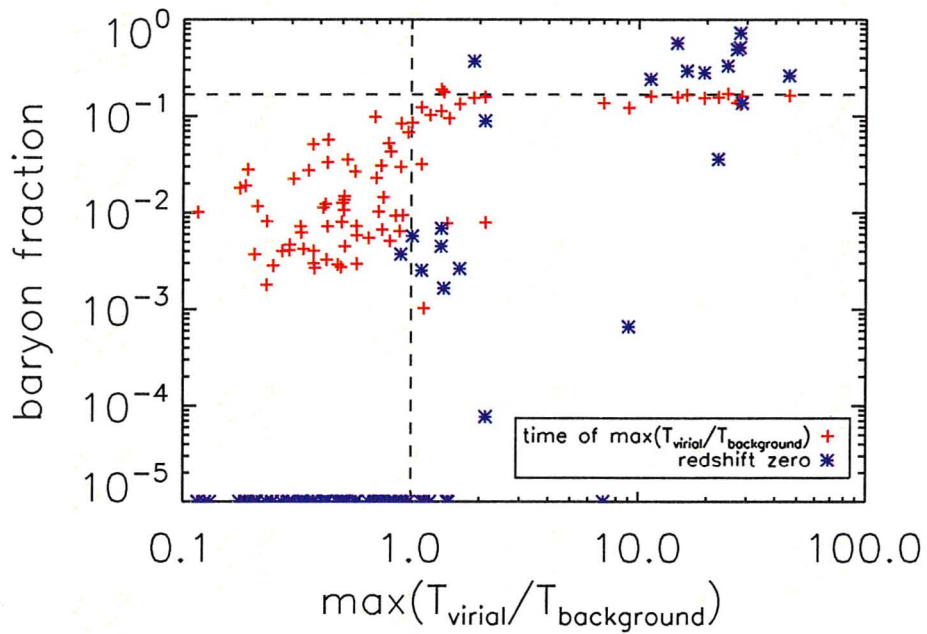


Figure 4.5: The baryon fraction versus the maximum ratio between the virial and background gas temperatures that a subhalo ever obtains over its lifetime in g15784. The horizontal black line represents the cosmic mean, 0.17, while the vertical black line separates the subhalos who achieved a  $T_{\text{vir}}$  higher than the background gas temperature on the right, with those that did not on the left. With one exception, every subhalo that is luminous at  $z = 0$  is to the right of the vertical line.

never identified most subhalos early enough to study them both before and after the UV background turns on. Our only means of peering back in time is to look at the behavior of the background gas because each of these gas particles begins right beside its dark matter twin. If the UV heats a gas twin particle too much then it cannot be drawn into the gravitational potential of the dark matter twin afterwards. We defined the UV loss for each subhalo as the mass of background gas that never joined it.

## 4.2 Tidal Stripping

Next, we examine mass loss due to tidal forces. This is the only force that can affect dark matter and stars along with the gas, while the UV background, stellar feedback, and ram pressure stripping simply cleave gas from dark matter. The subhalo's tidal radius is the place at which its self gravity is less than the tidal force of the host galaxy (e.g. Hayashi et al., 2003). We determine the amount mass lost due to tides using the tidal radius. Due to Newton's Theorem, assuming spherical symmetry, one need only consider the mass interior to a given particle. The gravitational force on the particle from inside the orbit of the particle is

$$F_{subhalo} = \frac{GM_{subhalo}(r)m_{particle}}{r^2} \quad (4.2)$$

where  $r$  is the distance from the particle to the centre of its subhalo,  $m_{particle}$  the mass of the particle, and  $M_{subhalo}(r)$  is the subhalo mass interior to  $r$ . The tidal force that the particle feels from the host, if the host galaxy is

approximated by a point mass, is the differential pull between the position of the particle in the subhalo and at the centre of the subhalo:

$$\delta F_{tidal} = \frac{-2GM_{host}m_{particle}r}{R_{host}^3} \quad (4.3)$$

where  $R_{host}$  is the distance between the subhalo and the host, and  $M_{host}$  is the mass of the host. Therefore, the condition for which the particle feels a greater tidal force than gravitational from its own subhalo is given by:

$$\frac{M_{subhalo}(r)}{r^3} < \frac{2M_{host}}{R_{host}^3} \quad (4.4)$$

A particle that passes this test qualifies for tidal stripping.

Figure 4.6 shows an example of a subhalo being tidally stripped of its gas. What is apparent are the tidal arms that stretch out due to the tides. Additionally, material is stripped off the outside first before the material on the inside.

### 4.3 Ram Pressure Stripping

One of the difficult aspects of this study is that the mass loss mechanisms involve the interaction between two gas phases with significantly different properties. Ram pressure stripping as analyzed by Gunn & Gott (1972) was applied to galaxies in falling into clusters, which happens when the pressure of the intracluster medium exceeds the force per area that holds the gas within the galaxy. In recent years ram pressure stripping has been applied to the situation of dwarf galaxies falling through the medium towards their hosts to help solve the missing satellites problem. Though Agertz et al. (2007) showed that

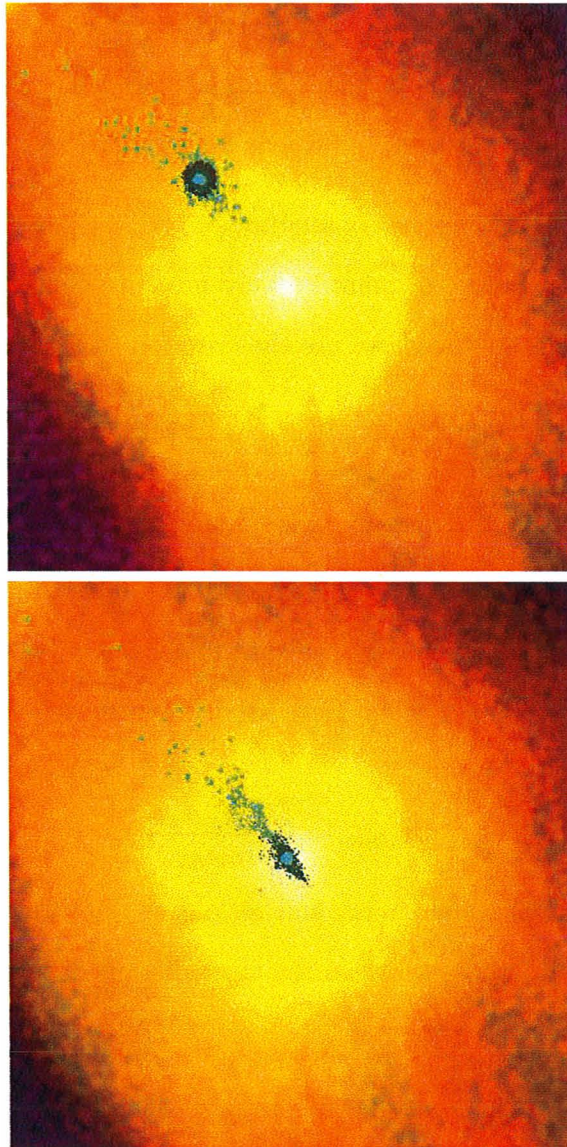


Figure 4.6: How tidal stripping removes gas from a  $2.0 \times 10^8 M_{\odot}$  subhalo between redshift 1.0 (top) and 0.8 (bottom). The dark matter (dark green), gas (light green) and stars (turquoise) are marked at the time of maximum mass, while the lower layer in brown is the subhalo at the present output. Note how the tidal stripping has already begun at redshift 1.0, and by redshift 0.8 the tidal tail is prominent. The dark matter has been compressed, while the stars sit more safely in the centre of the subhalo. The background colours are dark blue (colder,  $10^{1.5}K$ ) through to white (hotter,  $10^7K$ ) of the temperature of the surrounding gas in the high resolution region.

SPH has trouble modelling ram pressure stripping when the Kelvin-Helmholtz time is important, Mayer et al. (2006) showed that SPH works well when the dynamical time is shorter than the Kelvin-Helmholtz time.

We do a classical ram pressure analysis to see how close these simulations come to reality. In order to quantitatively measure the effect ram pressure stripping has on our subhalos, we use the criterion from Grebel et al. (2003):

$$P_{ram} \sim \rho_{hhg} v_{subhalo}^2 > \frac{\sigma_{subhalo}^2 \rho_{gas}}{3} \quad (4.5)$$

where  $P_{ram}$  is the ram pressure,  $\rho_{IGM}$  is the density of the hot halo gas around the subhalo,  $v_{subhalo}$  is the velocity of the subhalo relative to the host galaxy,  $\sigma_{subhalo}$  is the velocity dispersion of the gas in the subhalo,  $\rho_{gas}$  is the average density of the gas in the subhalo. Here we defined the velocity of the subhalo dispersion by

$$\sigma_{subhalo}^2 = \frac{3}{5} \frac{GM_{subhalo}}{R_{subhalo}} \quad (4.6)$$

where  $M_{subhalo}$  is the subhalo mass, and  $R_{subhalo}$  is the subhalo radius, defined as the maximum difference between the most distant of the subhalo particles and the subhalo centre of mass.

In order to measure the gas density around each subhalo, we computed the average density of the  $n^{th}$  nearest gas particles, where  $n$  is twice the number of particles in the subhalo to a maximum of 4000. The density and temperature structure of the gaseous halo of g15784, through which the subhalos pass, is shown in Figure 4.7 with substructure removed. A power law of slope  $-2.2$  is shown for reference.

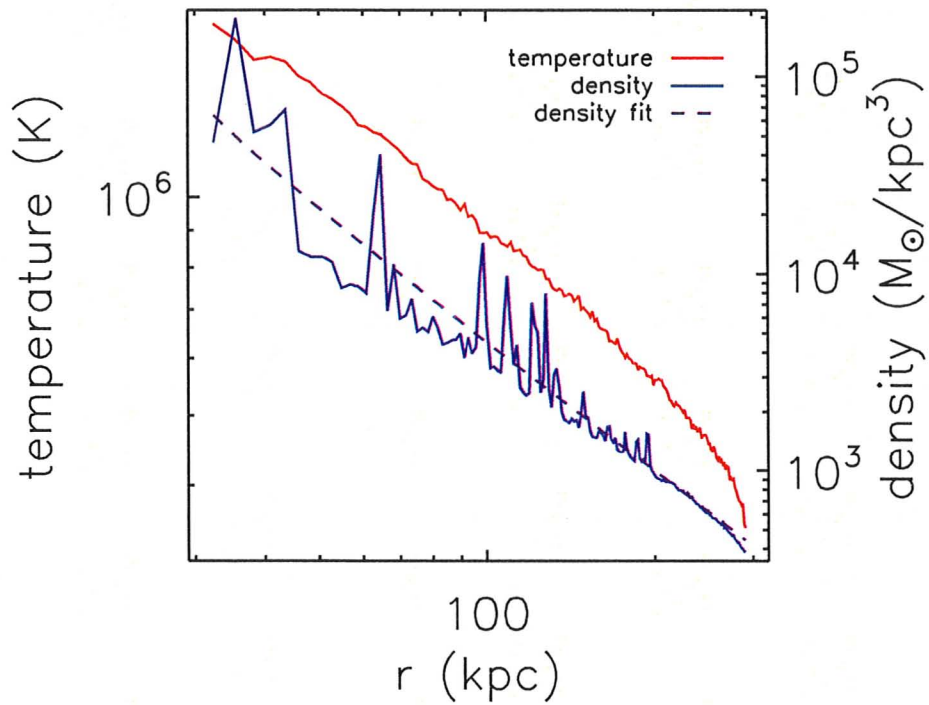


Figure 4.7: The gas temperature (red) and density (blue) profile of g15784 for the outer disk at  $r \geq 30\text{kpc}$ , with the density fit to a power law  $\rho \propto r^{-2.2}$  (dashed purple).

For the outputs in which the ram pressure exceeds the pressure in the subhalo, we define every gas particle that leaves in that output as leaving due to ram pressure stripping, with the exception of those that qualified for stellar feedback (§4.4).

However, we also generated movies of twelve low-mass subhalos and visually inspected them by eye to see if it was ram pressure stripping or tidal stripping that removed their gas. Figure 4.8 gives an example of a ram pressure-stripped subhalo. When some subhalos approach the host galaxy a burst of intergalactic hot gases washes past the subhalo and as this occurs, the subhalo gas and dark matter separate cleanly, the gas maintaining the shape of the dark matter for a few outputs. Tidal stripping pulls the gas away from the subhalo in distorted streams in opposite directions. Typically, ram pressure stripping occurs farther out from the host than tidal stripping.

We found that our definition for ram pressure stripping was much too weak and did not work in cases where ram pressure stripping was clearly happening in the visualization. This could be an effect of the simulation or resolution, and accordingly to compensate we varied the ram pressure stripping estimate by several different factors and found that increasing it by a factor of 10 yields sensible results. Figure 4.9 gives gas and ram pressure versus time for two subhalos, showing the difference the factor of 10 makes in increasing the ram pressure to be comparable with the subhalo's pressure where appropriate. In future, a comparison of higher-resolution simulations, as well as grid codes, to ours would be useful to see if they can exhibit ram pressure stripping.

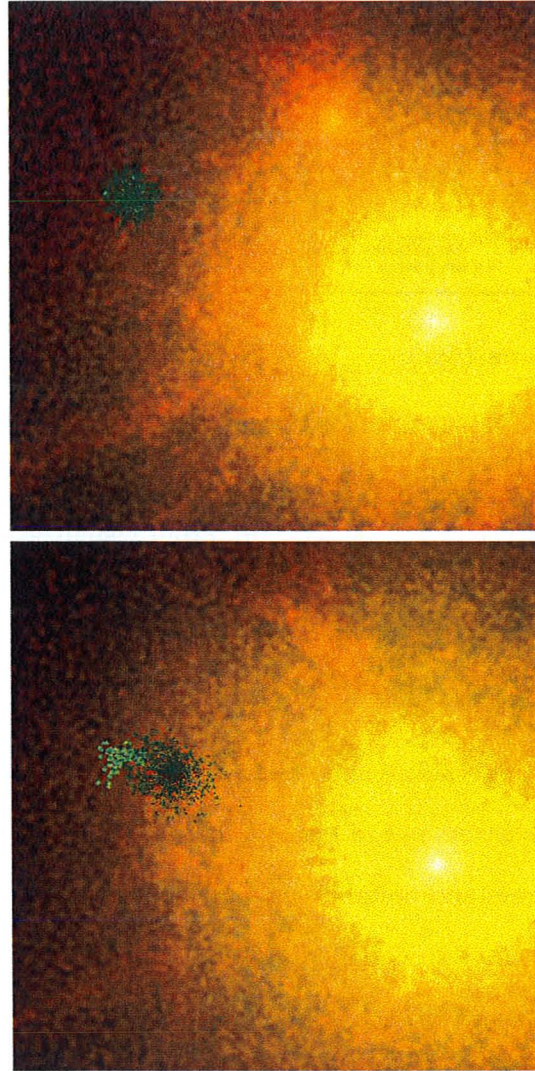


Figure 4.8: How ram pressure stripping removes gas from a  $1.7 \times 10^9 M_{\odot}$  subhalo between redshift 0.26 (top) and 0.16 (bottom). The dark matter (dark green), gas (light green) and stars (turquoise, none present here) are marked at the time of maximum mass, while the lower layer in brown is the subhalo at the present output. Ram pressure stripping has affected this subhalo, removing all of the gas it processed at the time of maximum mass, but without strengthening the ram pressure stripping diagnosis by a factor of 10 the individual gas particles would not be marked as ram pressure stripped. The background colours are dark blue (colder,  $10^{1.5} \text{K}$ ) through to white (hotter,  $10^7 \text{K}$ ) of the temperature of the surrounding gas in the high resolution region.

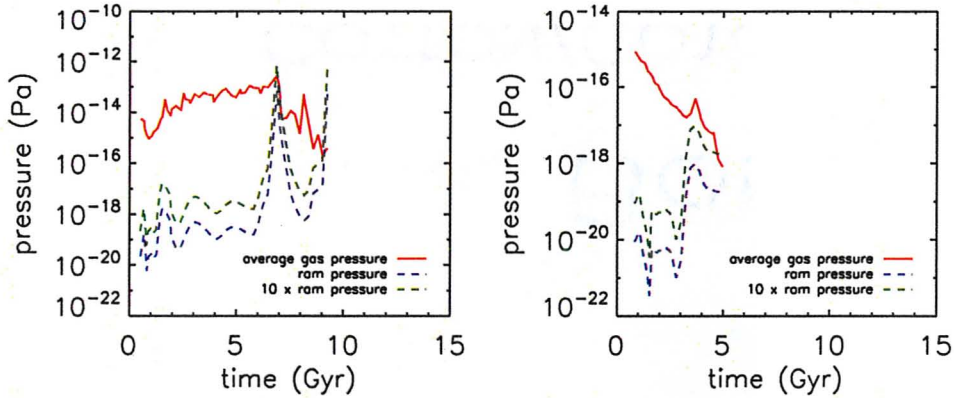


Figure 4.9: Pressure versus time for the subhalos sh4 (Figure 4.2) and sh7 (Figure 4.3) in g15784. Internal pressure is given by the solid red line, ram pressure from the hot halo gas is the blue dashed line, and ram pressure strengthened by a factor of 10 is the green dashed line. From visualization of the subhalos, sh4 was mostly affected by some ram pressure and later tides, while sh7 was affected largely by ram pressure stripping.

## 4.4 Stellar Feedback

Feedback from supernovae and stellar-driven winds have long been candidates for blowing baryons out of dwarf galaxies, which were observed to have low surface brightness and metallicities. Supernovae can release large amounts of energy into the inter-stellar medium (ISM), enough to affect the smaller dwarf galaxies. Larson (1974) found that lower mass galaxies would lose a higher fraction of their gas from supernovae, while Dekel & Silk (1986) showed that low mass is crucial in order for the first generation of supernovae-driven winds to cause galaxy-wide gas loss. Later observations showed gas in the act of being driven out of dwarf galaxies (Martin, 1996; della Ceca et al., 1996), and computer simulations supported these findings. Mac Low & Ferrara (1999) found that interstellar gas could only be ejected in galaxies lower than  $10^6 M_{\odot}$ . The Dekel & Woo (2003) simulations find that supernovae do indeed increase

the mass-to-light ratio for lower-mass galaxies, but also that stellar feedback is not enough on its own to explain the missing satellites problem.

The signature of stellar feedback in our MUGS simulations is that a gas particle has its cooling turned off as well as a metallicity increase, which allows it to maintain its high temperature due to the stellar energy release. When it gains sufficient kinetic energy, it can escape the gravitational potential of the subhalo. We attributed gas loss due to stellar feedback as when gas particles had their cooling turned off in the output before they left their subhalo. This is a conservative estimate since outputs were limited to approximately one every 100 to 200 Myr. Cooling is typically shut off for 50 Myr, so some particles may have had their cooling turned off in between outputs prior to ejection, but we were unable to detect these events.

There may have been cases where gas directly heated by stellar feedback acquired sufficient pressure to push out different gas, a process called “mass-loading”. This is common in dwarf galaxies (Dalla Vecchia & Schaye, 2008). We may have found stellar feedback particles to have not been removed due to stellar feedback when stellar feedback could have also enabled another mechanism like ram pressure stripping. Therefore, our stellar feedback category is under-represented given the results found with g5664 in §3.2, with particles truly affected by it probably getting mislabelled as ram pressure stripping or tidal stripping. §4.5 will show a large number of unclassified gas particles in some cases, and we suspect many of these might in fact be due to stellar feedback despite our labelling method being ineffective for it. We also tried labelling the subhalos that had their cooling turned off in the timestep after

ejection, and then either the timestep before or the timestep after ejection, and this had little difference in our numbers.

## 4.5 A Combination of Mechanisms

Using all the just described techniques, we followed the entry and exit of each particle from the subhalos to determine how the halos were built and how they lost their matter.

One confounding effect happened when subhalos passed their pericentre. The halos would temporarily accrete a small quantity of gas and quickly lose it, possibly a numerical effect. This is particularly visible in the last pericentre of sh3 in Figure 4.1. Because of this, we did not count mass loss of particles that entered and left subhalos after they reached their maximum mass.

Some particles left the subhalo more than once. In order avoid double counting, we only counted the last method by which a particle entered or left its subhalo. We noted which gas particles were converted into stars, so that we could identify what portion of the gas mass decrement was due to star formation and what portion was due to gas leaving the halo. The loss of many of particles could not be classified, so mass loss is often classified as “other”.

Figures 4.10 to 4.12 show the evolutionary history of massive subhalos (sh1 to sh3), Figures 4.13 to 4.15 show medium to low mass subhalos that had formed stars at some point (sh4 to sh6), and Figures 4.16 to 4.18 show medium to low mass dark subhalos that never formed stars (sh7 to sh9). These histories are coloured to indicate cumulative gas lost due to each of the mechanisms

described above: UV ionisation, tidal stripping, ram pressure stripping and stellar feedback. They also show the amount of gas and stars in the current timestep.

Most of the gas in the most massive subhalos sh1, sh2 and sh3 turn into stars quickly, leaving only a small fragment of gas left. Any categorized gas that is lost is usually due to tidal stripping with some stellar feedback. sh2 is the only one that also shows significant star loss, likely due to its multiple close passages to the host galaxy, seen in Figure 4.1.

The medium and low mass subhalos sh4, sh5, and sh6 show quickly-risen spikes in their gas content, the fraction of their maximum mass reaching 0.15 quickly, similar to the massive halos sh2 and sh3. However, sh4, sh5, and sh6 do not form stars with the same efficiency, leaving the gas vulnerable to quick stripping. There is more stellar feedback labelled in these subhalos too, showing how lower mass makes a subhalo more vulnerable to having its gas ejected due to stellar feedback. sh4 shows ram pressure stripping to be on par with tides, while tides become more important in sh5 and tides are the most important in sh6 with no ram pressure showing. As well, a higher percentage of stars are stripped in these halos as oppose to the massive ones sh1 to sh3.

The situation for the medium and low mass subhalos that never form stars, sh7, sh8 and sh9, is that the vast majority of their gas was removed due to the UV ionisation. sh7 and sh9 lose the rest due to ram pressure stripping, while in sh8 ram pressure stripping and tidal stripping take equal precedence.

Figure 4.19 shows the fraction of every subhalo's maximum mass that is lost due to each mechanism at redshift zero. These mass loss fractions are plotted

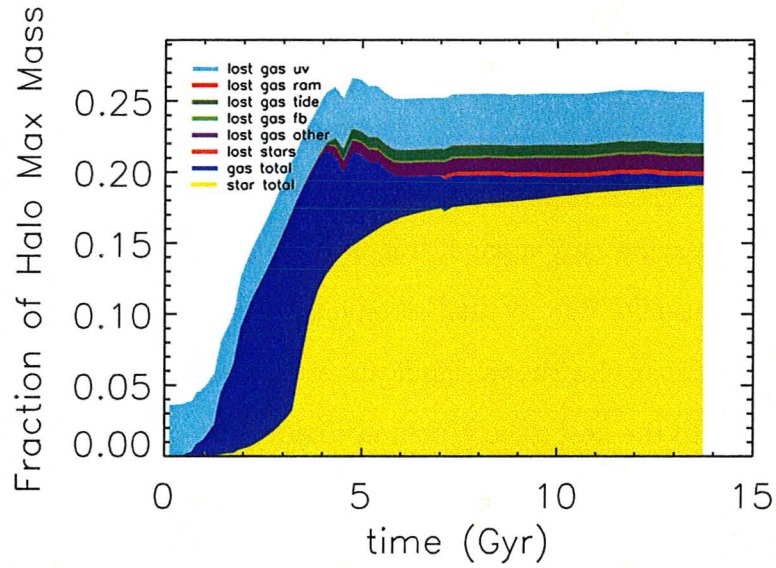


Figure 4.10: Mechanisms for baryon loss over time for the massive subhalo sh1 (maximum mass:  $1.1 \times 10^{10}M_{\odot}$ , final mass:  $7.1 \times 10^9M_{\odot}$ ), from Figure 4.1.

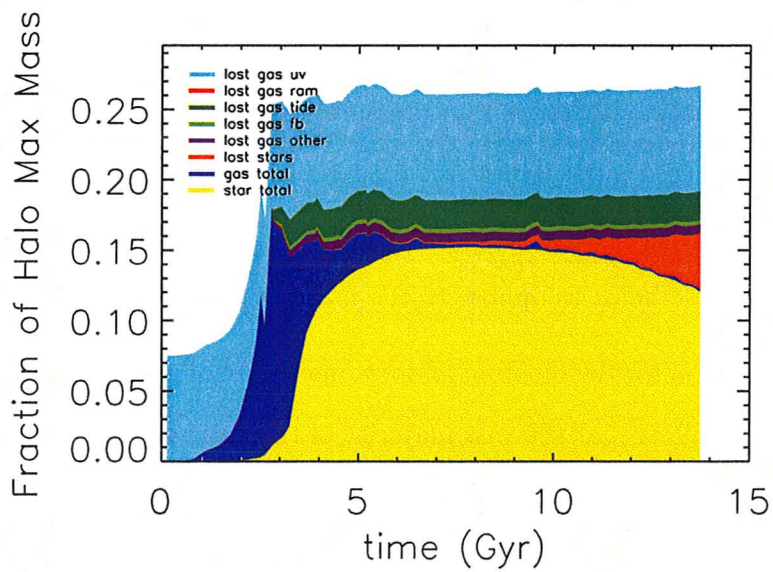


Figure 4.11: Mechanisms for baryon loss over time for the massive subhalo sh2 (maximum mass:  $1.4 \times 10^{10}M_{\odot}$ , final mass:  $2.3 \times 10^9M_{\odot}$ ), from Figure 4.1.

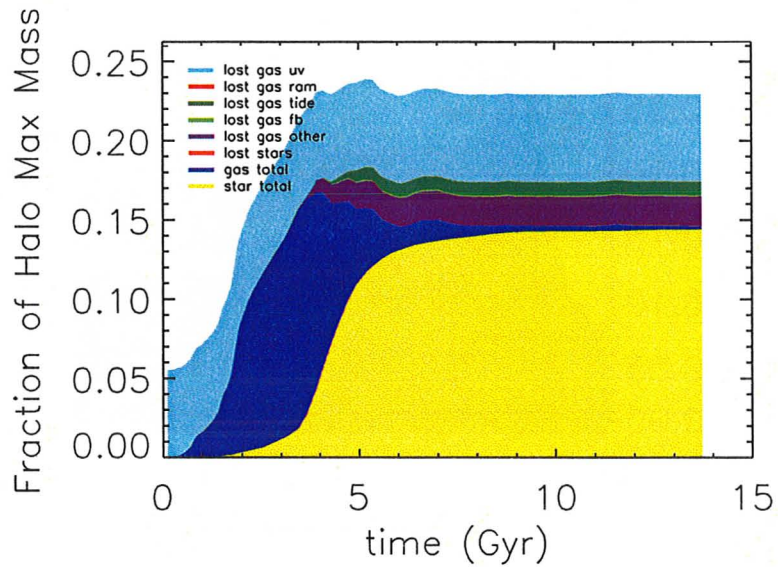


Figure 4.12: Mechanisms for baryon loss over time for the massive subhalo sh3 (maximum mass:  $7.4 \times 10^9 M_{\odot}$ , final mass:  $3.9 \times 10^9 M_{\odot}$ ), from Figure 4.1.

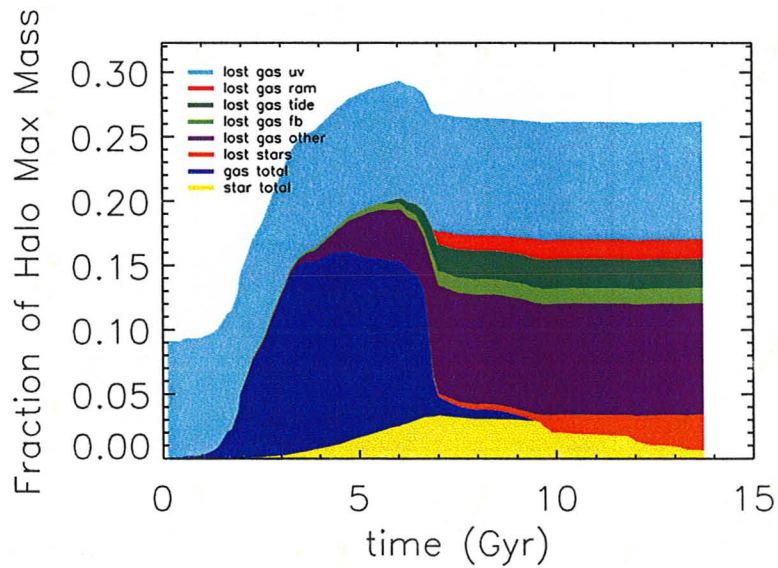


Figure 4.13: Mechanisms for baryon loss over time for the luminous medium mass subhalo sh4 (maximum mass:  $4.2 \times 10^9 M_{\odot}$ , final mass:  $2.0 \times 10^8 M_{\odot}$ , from Figure 4.2.

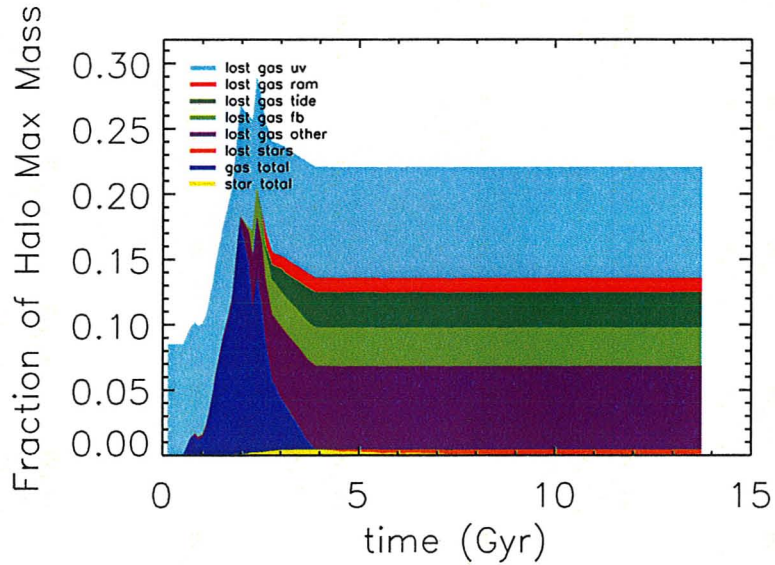


Figure 4.14: Mechanisms for baryon loss over time for the luminous low mass subhalo sh5 (maximum mass:  $1.2 \times 10^9 M_{\odot}$ , final mass:  $8.0 \times 10^7 M_{\odot}$ ), from Figure 4.2. It has managed to retain stars at redshift zero, but they are not numerous enough to show up well on this plot.

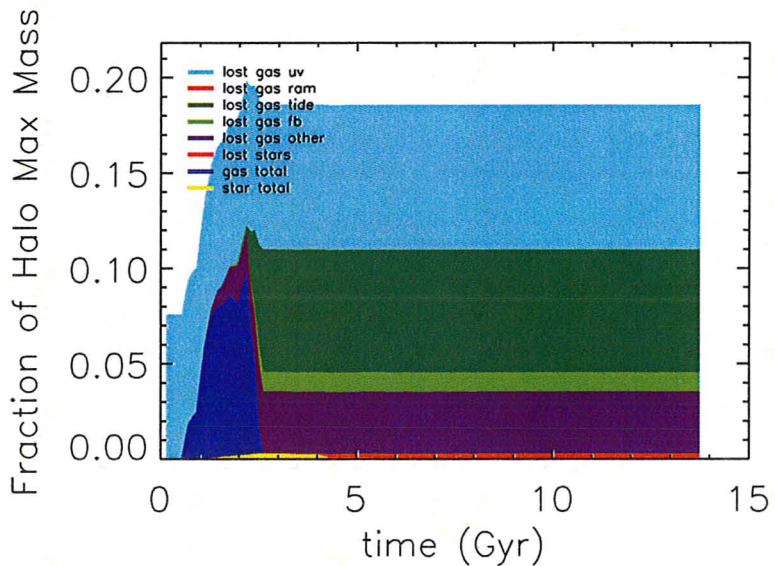


Figure 4.15: Mechanisms for baryon loss over time for the dark low mass subhalo sh6 (maximum mass:  $8.3 \times 10^9 M_{\odot}$ , final mass:  $6.9 \times 10^7 M_{\odot}$ ), from Figure 4.2. This subhalo formed stars, but they got stripped and so it ended up as a dark satellite.

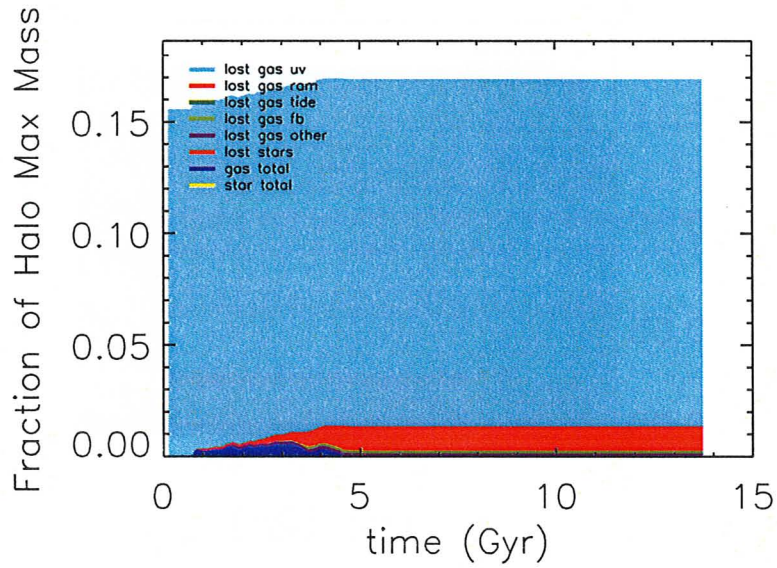


Figure 4.16: Mechanisms for baryon loss over time for the medium mass dark subhalo sh7 (maximum mass:  $1.2 \times 10^9 M_{\odot}$ , final mass:  $7.2 \times 10^8 M_{\odot}$ ), from Figure 4.3.

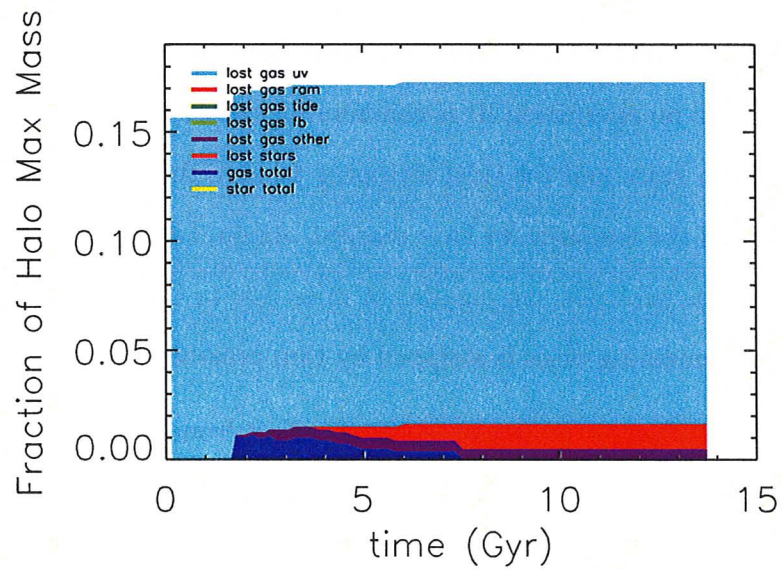


Figure 4.17: Mechanisms for baryon loss over time for the medium mass dark subhalo sh8 (maximum mass:  $1.5 \times 10^8 M_{\odot}$ , final mass:  $1.2 \times 10^8 M_{\odot}$ ), from Figure 4.3.

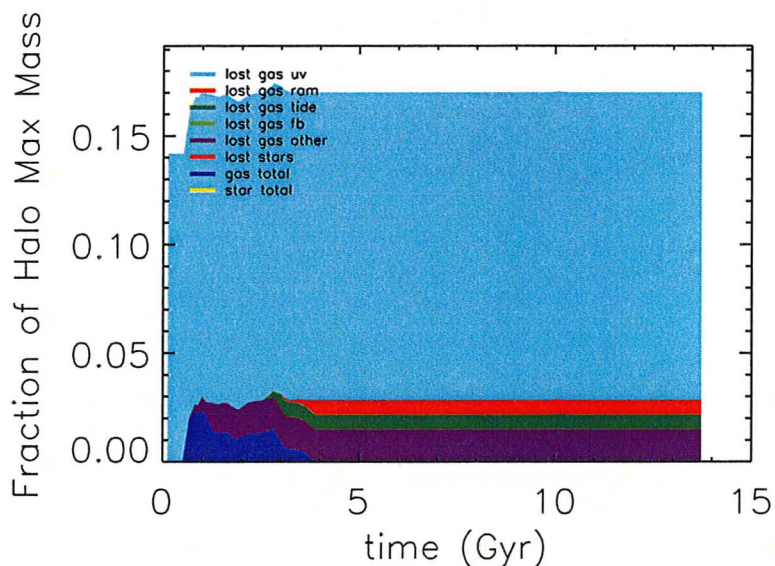


Figure 4.18: Mechanisms for baryon loss over time for the low mass dark subhalo sh9 (maximum mass:  $4.8 \times 10^8 M_\odot$ , final mass:  $9.5 \times 10^7 M_\odot$ ), from Figure 4.3.

as a function of maximum mass rather than final mass because the sequence appears much cleaner. Figure 4.19 shows that the massive subhalos in Figures 4.10 to 4.12 are no aberration. It is common for the most massive subhalos to efficiently form stars and for tidal stripping to play the most important role in mass loss, of the methods we have marked. Again, following Figures 4.16 to 4.18, lower mass subhalos lose significant mass due to UV ionisation and then much of the remaining mass is stripped by ram pressure.

Figure 4.19 does not show a significant effect from stellar feedback, even though the simulations of g5664 described in §3.2 indicated that there would be on the medium mass halos. Since we do not see this, our method of classifying mass loss as stellar feedback is incomplete. It is possible that much of the “other” category is stellar feedback. In the subhalos that form stars but are less

massive (sh4, sh5, sh6), the “other” category spikes right when star formation begins, but before the subhalos infall towards the host when tidal and ram pressure stripping are important. The fact that the “other” category is smaller in the massive subhalos (sh1, sh2, sh3) where stellar feedback is not strong enough to push out gas, and the lower mass subhalos that never form stars (sh7, sh8) supports this conclusion. The “other” category is still strong in sh9 however, and in Figure 4.19 there is one subhalo of mass greater than  $10^{10}M_{\odot}$  with significant “other”, and so the “other” category correlating to stellar feedback might not be true in every case.

There is a dichotomy of evolutionary scenarios apparent in Figure 4.19 between high mass satellites that form stars efficiently and the lower mass halos that form very few stars. The division is at  $\sim 2.0 \times 10^9 M_{\odot}$ . This distinction is not apparent when the satellites are classified by their final mass since Figure 3.2 shows the populations of baryonless and luminous subhalos overlap in terms of total mass at  $z = 0$ . We will expand on this in Chapter 5.

## 4.6 Baryon Excess in Massive Halos

For the lower mass subhalos, the amount of mass lost adds up nearly to the cosmic baryon fraction, in part because our analysis relied on pairing dark and gas particles. However, all the higher mass subhalos form more stars than the cosmic baryon fraction. To understand why the higher mass subhalos form so many stars, we investigated the origin of these stars. Figure 4.20 shows the mass evolution of sh1, which contains more than the cosmic baryon fraction in stars at redshift zero. The mass evolution is divided into categories based on

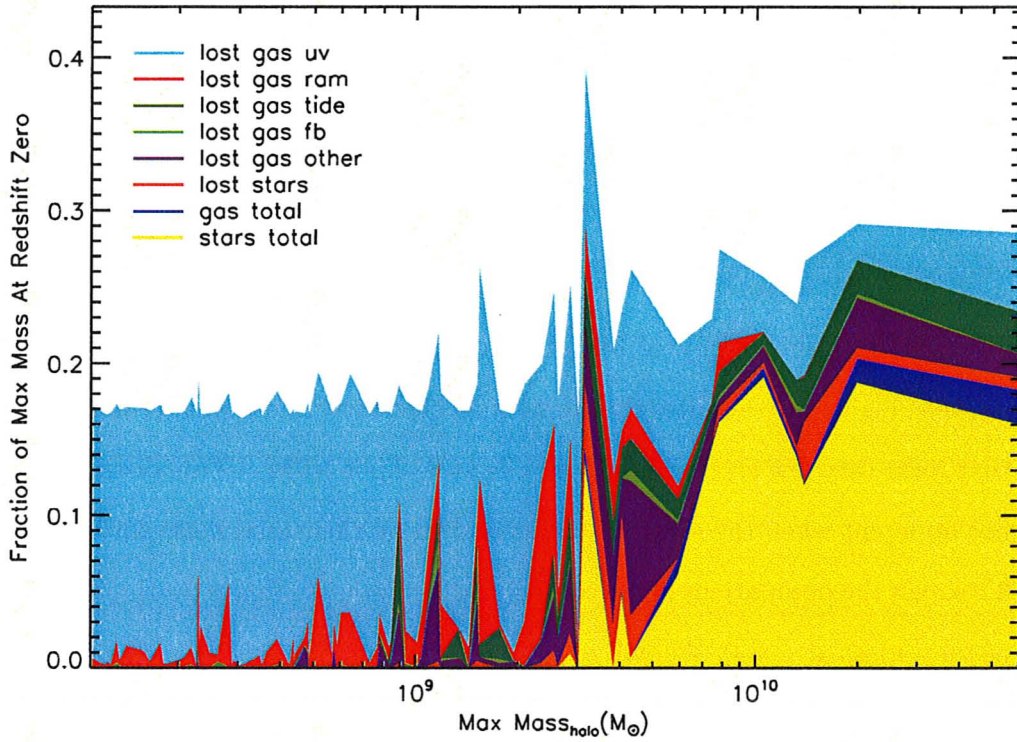


Figure 4.19: Mechanisms for baryon loss at  $z = 0$  for all subhalos, as a function of the maximum mass that a subhalo was able to achieve. The various loss mechanisms are cumulative over time, while the total gas and stars are for the current time. All values are a fraction of the subhalo's maximum mass. The luminous subhalos show an excess of baryons over their lifetime, above the cosmic mean of 0.17. The cutoff between luminous and dark satellites happens at about  $2.0 \times 10^9 M_{\odot}$ .

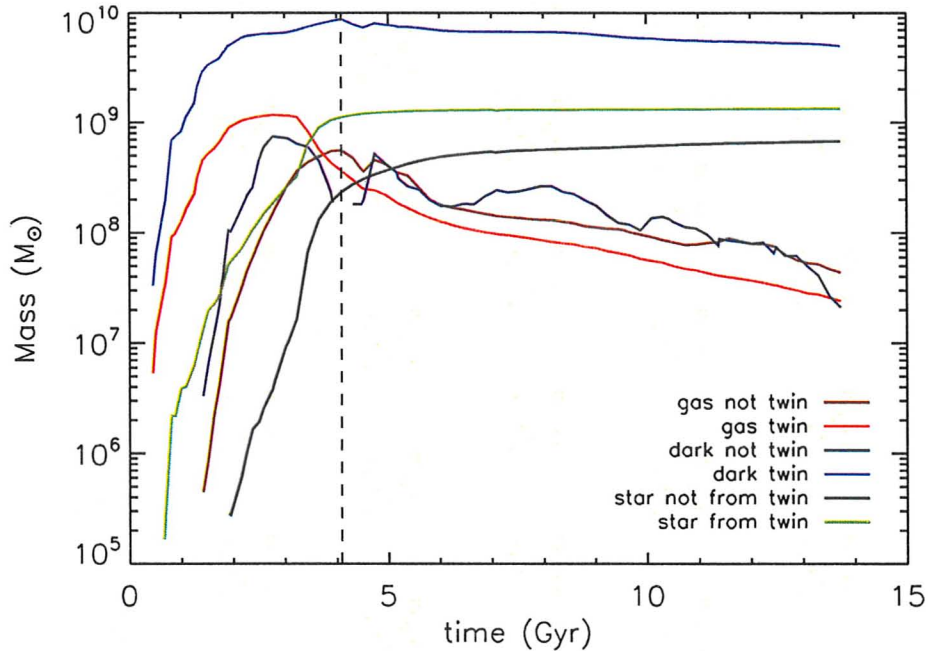


Figure 4.20: Time evolution of the matter in subhalo sh1 (Figure 4.1), broken down into dark matter present (considered to be a twin) and not present (considered to be not twin) at the time of maximum mass, gas twinned or not from the dark matter present at the time of maximum mass, and stars that did form from the gas twins and those that did not. The dashed vertical line is the time of maximum mass. Despite the difference in magnitudes between the twin and non-twin dark matter, the twin and non-twin gas particles are comparable, suggesting that the dark matter draws on gas outside its region of origin.

whether the particles were twins of the dark matter present at the maximum mass. While most of the stars formed from gas that was a twin of this dark matter, almost a tenth came from gas that was not twinned to dark matter present at the time of maximum mass. We tried to find out if any of the gas that formed stars were twins of dark matter that was part of the halo than maximum mass and found out that it did not.

We followed the evolution of this extra gas and found that each massive subhalo accreted gas from a region much wider than where the dark matter was accreted from. The non-twin gas that accretes is marked green in Figure 4.21 compared to the subhalo in brown. While this accretion could be an artifact of overly-efficient gas cooling in simulations, it could also be unique to subhalos that orbit in a high density region where the supply of gas could cool onto the subhalo. Higher mass subhalos tend to form stars early, consuming the gas that once gave pressure support to the subhalo. This causes the subhalo to draw on more gas from its surroundings, which in turn fuels a further cycle of star formation.

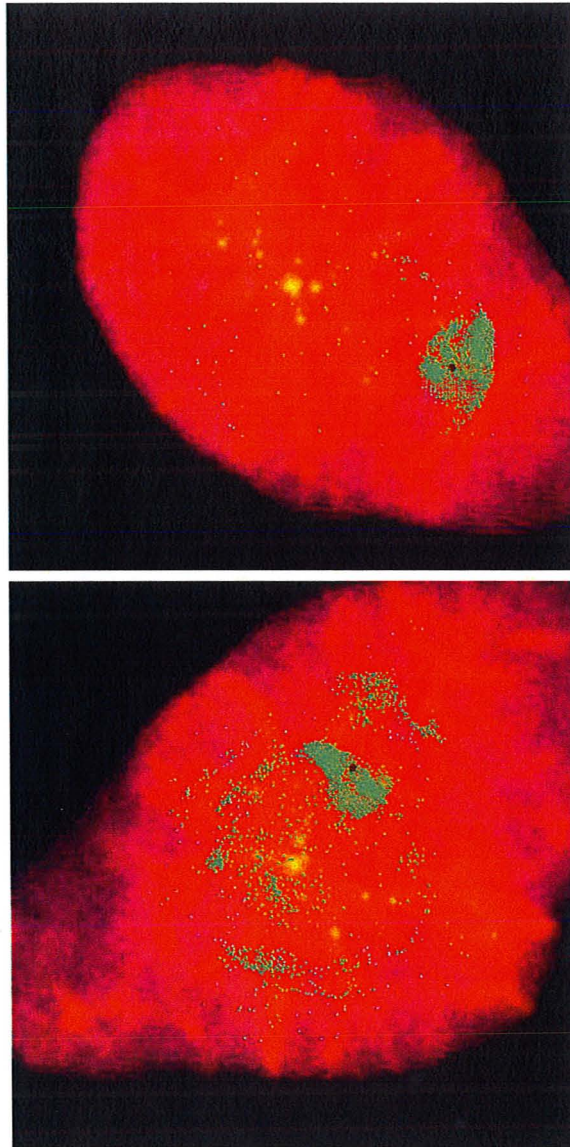


Figure 4.21: Snapshots at redshift 6 of the  $7.1 \times 10^9 M_{\odot}$  mass subhalo sh1 (top) and the  $2.4 \times 10^9 M_{\odot}$  mass subhalo sh2 (bottom), both from Figure 4.1. The subhalos are in brown, while light green is the gas that will produce all the non-twin stars that will end up in the subhalos. The gas will eventually converge into the subhalos. sh2 will end up in a tight orbit around the host, and hence the several shells of gas that it will draw upon. The background colours are dark blue (colder,  $10^{1.5}K$ ) through to white (hotter,  $10^7K$ ) of the temperature of the surrounding gas in the high resolution region.



## Chapter 5

# The Cutoff Between Luminous and Dark Satellites

Now that we have examined in detail the mass loss mechanisms for one particular galaxy, g15784, it is time to step back and see the entire picture again for more of galaxies provided by MUGS.

As we saw in Figure 4.19 the subhalos' maximum mass for g15784 is a means of determining if a satellite will be luminous or not at redshift zero. To see if this holds for other galaxies, we traced the histories of the satellites of six galaxies and in Figure 5.1 we plot the baryonic mass at redshift zero over the maximum mass versus the subhalos' maximum mass. Here we find that around  $2.0 \times 10^9 M_{\odot}$  in every single system there is a divide between luminous subhalos and dark according to maximum mass. Table 5.1 gives the largest value over all the dark satellites' maximum masses, and the smallest values of all the luminous satellites' maximum masses for each of these six galaxies. The maximum mass of dark satellites has never been heavier than  $2.8 \times 10^9 M_{\odot}$  and a luminous satellite's maximum mass has never been lighter than  $2.3 \times 10^8 M_{\odot}$ .

Although the dark satellites and luminous satellites do overlap slightly, meaning that the cutoff between luminous and dark is not a hard value, there seems to be a limit for both classes of satellites. This means that beyond these values, a subhalo's ultimate fate is determined, while in between a subhalo could end up being either dark or luminous, swayed by a host of additional factors, including the environment it is born in and the distance to its host galaxy. One caveat is that increasing simulation resolution could push this border downwards as the particle size decreases and lower baryon masses can become possible.  $\sim 10^9 M_{\odot}$  is presently about a thousand dark matter particles, the number needed for star formation (Christensen et al., 2010), and so clearly there is still room for higher resolution simulations to explore the border between luminous and dark satellites further.

To further illustrate why the maximum mass is more suitable and why the final mass is not, Figure 5.2 is given, showing the maximum mass versus the final mass for the satellite populations in each of the six galaxies. Clearly, a single value of maximum mass for a subhalo can become several values of final mass leading to a degeneracy. There might instead be several factors leading to this. One of these is pericentre of the orbit. Figure 5.3 shows the ratio of the final mass to the maximum mass for the subhalos in g15784 versus the minimum distance each subhalo passes to the host, coloured by mass-to-light ratio. For the subhalos that have no baryon particles, there is a clear trend where the ones that pass closer to the host tend to lose more mass since the time of their maximum mass. For the lowest mass-to-light ratio subhalos, the mass-loss penalty is lower per close distance to the host than for the dark subhalos. The subhalos of medium mass-to-light-ratio all tend to be relatively

Galaxy	Max Mass of Dark Satellite Max Mass ( $10^8 M_\odot$ )	Min Mass of Luminous Sat Max Mass ( $10^8 M_\odot$ )
g7124	8.3	5.0
g5664	24	2.3
g24334	27	3.2
g422	28	9.6
g3021	26	9.0
g15784	17	9.5

Table 5.1: The highest maximum mass a dark satellite ever has, and the lowest maximum mass a luminous satellites ever has within each of the six MUGS galaxies detailed. They are shown in order of increasing host mass as given in Table 2.4.

close to the host compared to the dark subhalos, possibly becoming luminous because they began in more gas-rich regions, but get stripped more than the lowest mass-to-light ratio subhalos.

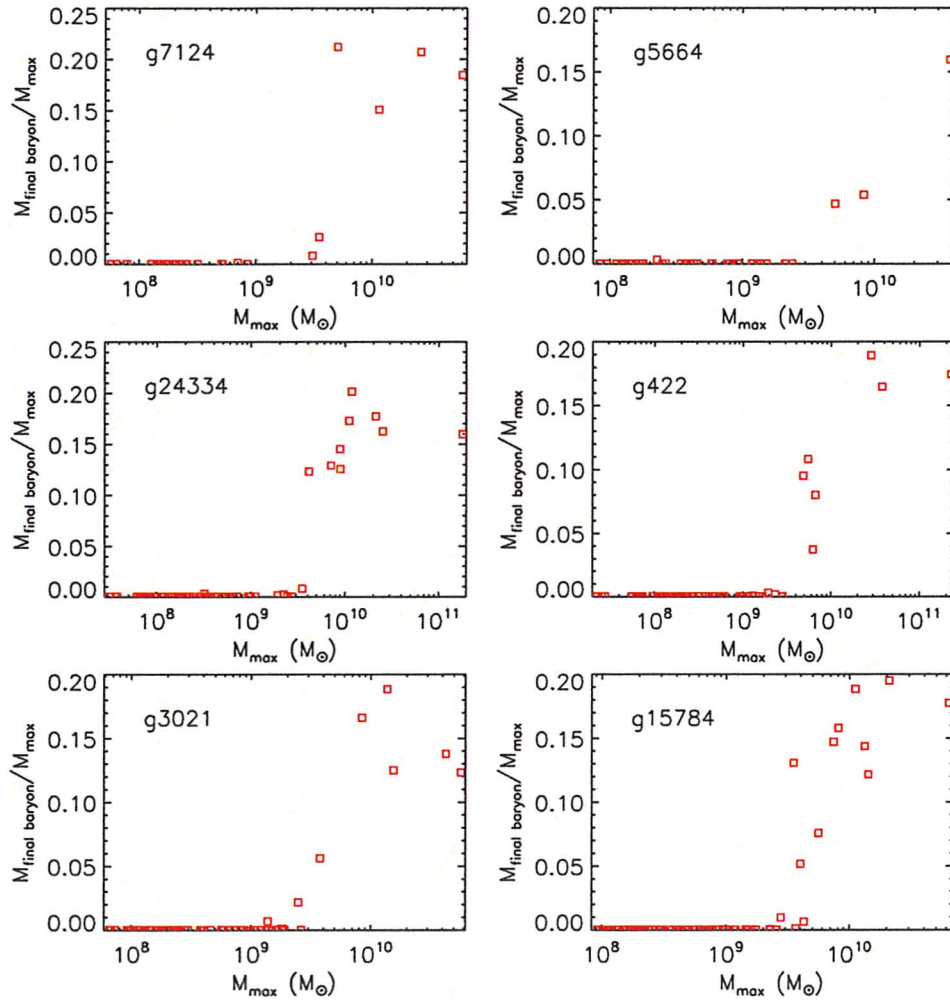


Figure 5.1: The baryon fraction at redshift zero of the maximum mass versus the subhalos' maximum mass, for six MUGS galaxies. They are shown in order of increasing host mass as given in Table 2.4.

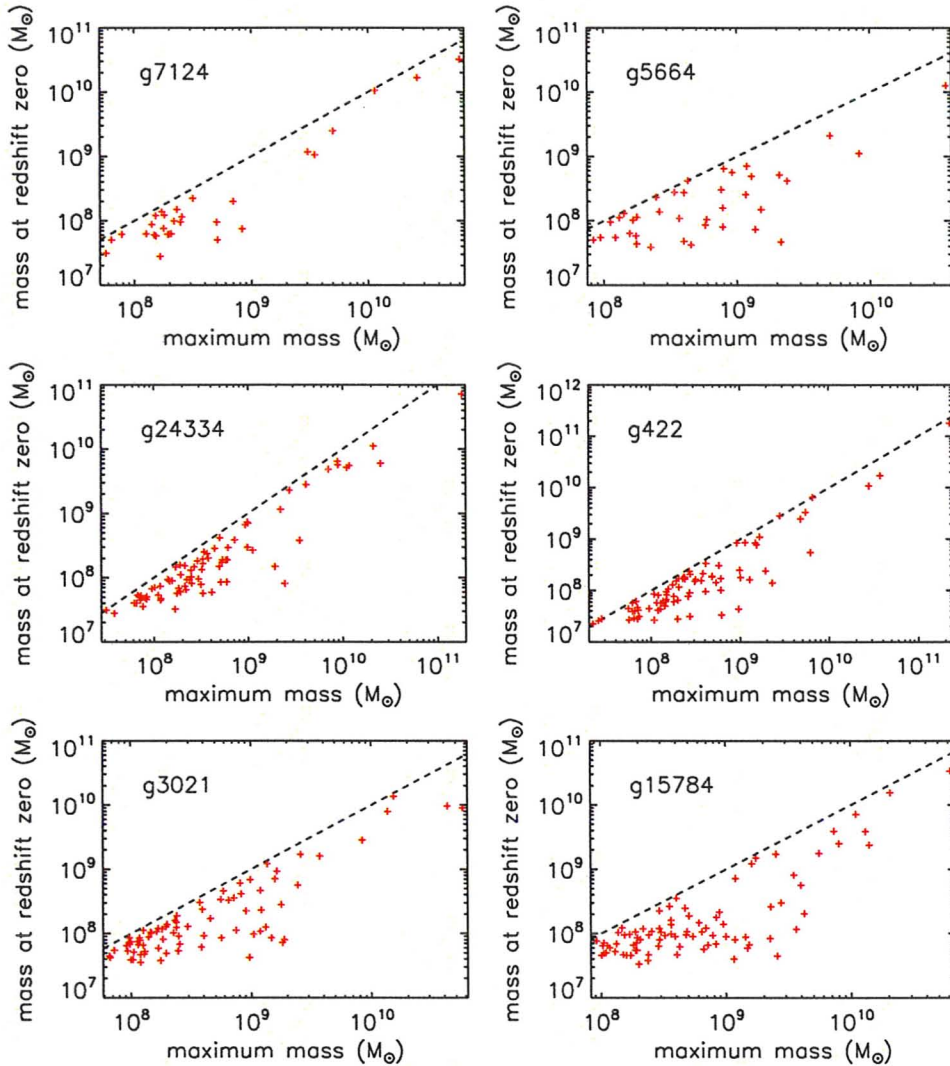


Figure 5.2: The subhalos' maximum mass versus their mass at redshift zero, for six MUGS galaxies. The dashed line represents the point at which the maximum and final mass are equal. Here it is clear that for any given value of maximum mass, there can be many satellites that end up with a range of final masses. They are shown in order of increasing host mass as given in Table 2.4.

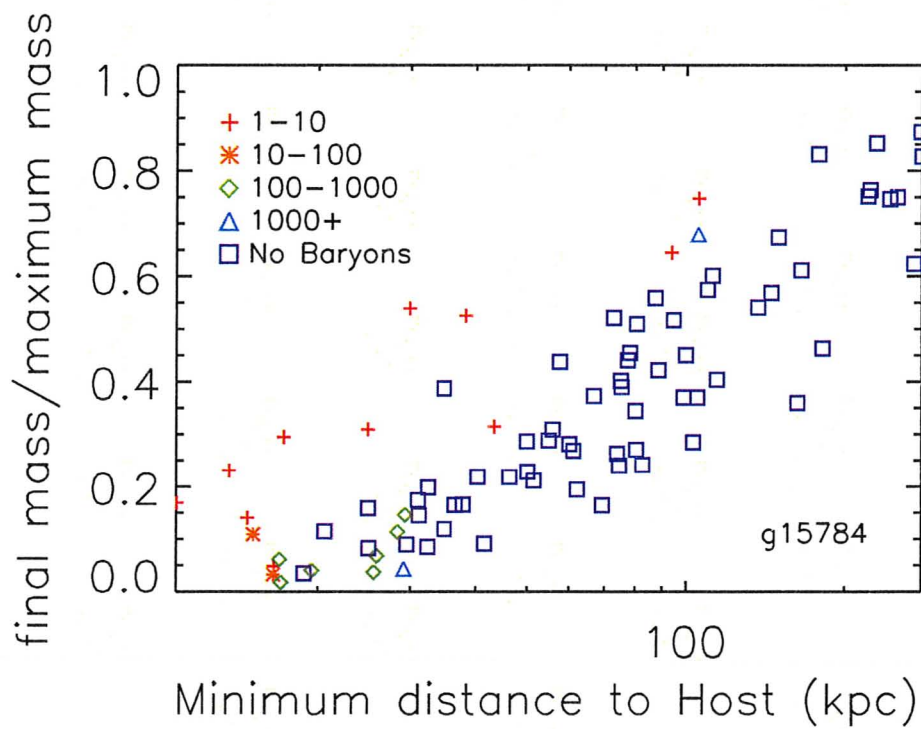


Figure 5.3: For the subhalo population of g15784, the ratio of maximum mass to final mass, versus the minimum distance to the host. The satellites are coloured according to mass-to-light ratio, and the lower bound in the legend is inclusive. The subhalo population without baryons shows a trend of losing more of their maximum mass the closer they pass to the host.

## Chapter 6

### Conclusions and Discussion

To gain insight into the missing satellites problem, we compared the satellite luminosity functions of fourteen host galaxies simulated as part of the MUGS project with observations of the Milky Way. The luminosity functions showed that each halo contained a large population of dark satellites, meaning that their luminosity functions match observations relatively closely for those with masses close to the Milky Way's. To understand the effects of feedback on the satellite luminosity function, we re-simulated the smaller galaxy g5664 ( $5.2 \times 10^{11} M_{\odot}$ ) twice, once without UV background and feedback, and once without feedback but with UV. The effect they had on the subhalo populations was significant. Both feedback and the UV background remove the subhalos' baryons very effectively.

Our total mass versus luminous mass relation for all galaxies reveal two populations: the dark satellites that have no luminous mass, and the luminous satellites, both of which have overlapping values of total mass. This overlap disagrees with many previous analytical predictions (Bullock et al., 2000; Peñarrubia et al., 2008) that at  $z = 0$  there is a mass cutoff that separates luminous from dark satellites, though it supports the numerical findings from

Strigari et al. (2007). In previous collisionless simulations, the determining effect of maximum mass was not apparent but this becomes much clearer in our simulations with baryons. Indeed, we have shown that the cutoff is a function of the maximum mass each subhalo is able to achieve over its lifetime, though there is a region in which a satellite could end up being luminous or dark. The highest maximum mass for a dark satellite was  $2.8 \times 10^9 M_{\odot}$  and the lowest maximum mass for a luminous satellite was  $2.3 \times 10^8 M_{\odot}$ .

High mass subhalos exhibited an interesting phenomenon, having more baryons than the cosmic fraction mostly in stars. We tracked the gas that created these stars to their origins and found that they were from regions far wider than the local region where the dark matter subhalo first accreted. Instead the gas was even picked up during the subhalo's orbit around its hot gaseous host. This might be due to the overcooling problematic to simulations, or enhanced baryonic accretion that is possible for subhalos in regions of high gas density.

We have also presented a comprehensive study of the mechanisms that strip the baryons off of subhalos for the galaxy g15784, and compared their varying strengths across subhalos of all masses. We defined criteria for loss due to the UV background, tidal stripping, ram pressure stripping, and stellar feedback.

In the end, our simulations show that there is no single smoking gun to explain how the dark satellites lost their gas. Instead, many mechanisms work in concert to expel it, and tend to be more effective closer to the host galaxy. The heating of the gas due to the UV background early in the Universe's lifetime prevents gas from ever significantly collecting in all but the most

massive of the early subhalos. The gas that the subhalos do have tends to be tidally stripped in the most massive subhalos and ram pressure stripped in the lower mass subhalos. The labelling system did not find enough stellar feedback, though it was most prominent in medium mass subhalos that did process stars at some point in their lives. This reveals a flaw in our direct particle-labelling method, given the results from g5664 which show that stellar feedback is very important in controlling the luminous subhalo population.

Future work in this area includes tracking where the baryons go once they leave their subhalos to see their importance in feeding the host galaxy. Refining the method of marking particles affected by stellar feedback, particularly by tracking the increase in metallicity in gas, is also key. Furthermore, we need to run convergence studies on how the resolution of a simulation could affect the mass cutoff limit between luminous and dark satellites, and look at this across more galaxies in the MUGS suite. Lastly, we would like to further study the enhanced gas accretion in massive subhalos.



## Bibliography

Agertz, O., Moore, B., Stadel, J., Potter, D., Miniati, F., Read, J., Mayer, L., Gawryszczak, A., Kravtsov, A., Nordlund, Å., Pearce, F., Quilis, V., Rudd, D., Springel, V., Stone, J., Tasker, E., Teyssier, R., Wadsley, J., & Walder, R. 2007, *MNRAS*, 380, 963

Alpher, R. A., Bethe, H., & Gamow, G. 1948, *Physical Review*, 73, 803

Astier, P., Guy, J., Regnault, N., Pain, R., Aubourg, E., Balam, D., Basa, S., Carlberg, R. G., Fabbro, S., Fouchez, D., Hook, I. M., Howell, D. A., Lafoux, H., Neill, J. D., Palanque-Delabrouille, N., Perrett, K., Pritchett, C. J., Rich, J., Sullivan, M., Taillet, R., Aldering, G., Antilogus, P., Arsenijevic, V., Balland, C., Baumont, S., Bronder, J., Courtois, H., Ellis, R. S., Filiol, M., Goncalves, A. C., Goobar, A., Guide, D., Hardin, D., Lusset, V., Lidman, C., McMahon, R., Mouchet, M., Mourao, A., Perlmutter, S., Ripoche, P., Tao, C., Walton, N., & SNLS Collaboration. 2005, in *Bulletin of the American Astronomical Society*, Vol. 37, *Bulletin of the American Astronomical Society*, 1176–+

Babcock, H. W. 1939, *Lick Observatory Bulletin*, 19, 41

Becker, R. H., Fan, X., White, R. L., Strauss, M. A., Narayanan, V. K., Lupton, R. H., Gunn, J. E., Annis, J., Bahcall, N. A., Brinkmann, J., Connolly, A. J., Csabai, I., Czarapata, P. C., Doi, M., Heckman, T. M., Hennessy, G. S., Ivezić, Ž., Knapp, G. R., Lamb, D. Q., McKay, T. A., Munn, J. A., Nash,

- T., Nichol, R., Pier, J. R., Richards, G. T., Schneider, D. P., Stoughton, C., Szalay, A. S., Thakar, A. R., & York, D. G. 2001, *AJ*, 122, 2850
- Belokurov, V., Zucker, D. B., Evans, N. W., Kleyana, J. T., Koposov, S., Hodgkin, S. T., Irwin, M. J., Gilmore, G., Wilkinson, M. I., Fellhauer, M., Bramich, D. M., Hewett, P. C., Vidrih, S., De Jong, J. T. A., et al. 2007, *ApJ*, 654, 897
- Blumenthal, G. R., Faber, S. M., Primack, J. R., & Rees, M. J. 1984, *Nature*, 311, 517
- Bond, J. R. & Szalay, A. S. 1983, *ApJ*, 274, 443
- Bullock, J. S., Dekel, A., Kolatt, T. S., Kravtsov, A. V., Klypin, A. A., Porciani, C., & Primack, J. R. 2001, *ApJ*, 555, 240
- Bullock, J. S., Kravtsov, A. V., & Weinberg, D. H. 2000, *ApJ*, 539, 517
- Christensen, C. R., Quinn, T., Stinson, G., Bellovary, J., & Wadsley, J. 2010, *ApJ*, 717, 121
- Dalal, N. & Kochanek, C. S. 2002, *ApJ*, 572, 25
- Dalcanton, J. J. & Hogan, C. J. 2001, *ApJ*, 561, 35
- Dalla Vecchia, C. & Schaye, J. 2008, *MNRAS*, 387, 1431
- Dall'Aglio, A., Wisotzki, L., & Worseck, G. 2009, ArXiv e-prints
- Dehnen, W., McLaughlin, D. E., & Sachania, J. 2006, *MNRAS*, 369, 1688
- Dekel, A. & Silk, J. 1986, *ApJ*, 303, 39

Dekel, A. & Woo, J. 2003, MNRAS, 344, 1131

della Ceca, R., Griffiths, R. E., Heckman, T. M., & MacKenty, J. W. 1996,  
ApJ, 469, 662

Dicke, R. H., Peebles, P. J. E., Roll, P. G., & Wilkinson, D. T. 1965, ApJ, 142,  
414

Efstathiou, G. 1992, MNRAS, 256, 43P

Einasto, J., Kaasik, A., & Saar, E. 1974, Nature, 250, 309

Fan, X., White, R. L., Davis, M., Becker, R. H., Strauss, M. A., Haiman,  
Z., Schneider, D. P., Gregg, M. D., Gunn, J. E., Knapp, G. R., Lupton,  
R. H., Anderson, Jr., J. E., Anderson, S. F., Annis, J., Bahcall, N. A.,  
Boroski, W. N., Brunner, R. J., Chen, B., Connolly, A. J., Csabai, I., Doi,  
M., Fukugita, M., Hennessy, G. S., Hindsley, R. B., Ichikawa, T., Ivezić, Ž.,  
Loveday, J., Meiksin, A., McKay, T. A., Munn, J. A., Newberg, H. J., Nichol,  
R., Okamura, S., Pier, J. R., Sekiguchi, M., Shimasaku, K., Stoughton, C.,  
Szalay, A. S., Szokoly, G. P., Thakar, A. R., Vogeley, M. S., & York, D. G.  
2000, AJ, 120, 1167

Ferguson, H. C. & Binggeli, B. 1994, A&A Rev., 6, 67

Ferland, G. J., Korista, K. T., Verner, D. A., Ferguson, J. W., Kingdon, J. B.,  
& Verner, E. M. 1998, PASP, 110, 761

Flores, R. A. & Primack, J. R. 1994, ApJ, 427, L1

Forman, W. & Jones, C. 1982, ARA&A, 20, 547

Freedman, W. L., Madore, B. F., Gibson, B. K., Ferrarese, L., Kelson, D. D., Sakai, S., Mould, J. R., Kennicutt, Jr., R. C., Ford, H. C., Graham, J. A., Huchra, J. P., Hughes, S. M. G., Illingworth, G. D., Macri, L. M., & Stetson, P. B. 2001, *ApJ*, 553, 47

Friedman, A. 1922, *Zeitschrift fur Physik*, 10, 377

Gallagher, III, J. S. & Wyse, R. F. G. 1994, *PASP*, 106, 1225

Gamow, G. 1948, *Physical Review*, 74, 505

Geha, M., Blanton, M. R., Masjedi, M., & West, A. A. 2006, *ApJ*, 653, 240

Governato, F., Mayer, L., Wadsley, J., Gardner, J. P., Willman, B., Hayashi, E., Quinn, T., Stadel, J., & Lake, G. 2004, *ApJ*, 607, 688

Governato, F., Willman, B., Mayer, L., Brooks, A., Stinson, G., Valenzuela, O., Wadsley, J., & Quinn, T. 2007, *MNRAS*, 374, 1479

Gramann, M. 1988, *MNRAS*, 234, 569

Grebel, E. K. 1997, in *Reviews in Modern Astronomy*, Vol. 10, *Reviews in Modern Astronomy*, ed. R. E. Schielicke, 29–60

Grebel, E. K., Gallagher, III, J. S., & Harbeck, D. 2003, *AJ*, 125, 1926

Gunn, J. E. & Gott, III, J. R. 1972, *ApJ*, 176, 1

Gunn, J. E. & Peterson, B. A. 1965, *ApJ*, 142, 1633

Guo, Q., White, S., Li, C., & Boylan-Kolchin, M. 2009, *ArXiv e-prints*

Guyot, M. & Zeldovic, Y. B. 1970, *A&A*, 9, 227

- Haardt, F. & Madau, P. 1996, *ApJ*, 461, 20
- Hayashi, E., Navarro, J. F., Taylor, J. E., Stadel, J., & Quinn, T. 2003, *ApJ*, 584, 541
- Henry, R. C. 1991, *ARA&A*, 29, 89
- Hunter, D. A. & Gallagher, III, J. S. 1985, *ApJS*, 58, 533
- Ikeuchi, S. & Ostriker, J. P. 1986, *ApJ*, 301, 522
- Jeans, J. H. 1902, *Royal Society of London Philosophical Transactions Series A*, 199, 1
- Kennicutt, R. C. 1998, *ApJ*, 498, 541
- Klimentowski, J., Lokas, E. L., Knebe, A., Gottlöber, S., Martinez-Vaquero, L. A., Yepes, G., & Hoffman, Y. 2010, *MNRAS*, 402, 1899
- Klypin, A., Kravtsov, A. V., Valenzuela, O., & Prada, F. 1999, *ApJ*, 522, 82
- Klypin, A., Zhao, H., & Somerville, R. S. 2002, *ApJ*, 573, 597
- Knollmann, S. R. & Knebe, A. 2009, *ApJS*, 182, 608
- Koposov, S., Belokurov, V., Evans, N. W., Hewett, P. C., Irwin, M. J., Gilmore, G., Zucker, D. B., Rix, H., Fellhauer, M., Bell, E. F., & Glushkova, E. V. 2008, *ApJ*, 686, 279
- Koposov, S. E., Yoo, J., Rix, H., Weinberg, D. H., Macciò, A. V., & Escudé, J. M. 2009, *ApJ*, 696, 2179
- Kravtsov, A. 2010, *Advances in Astronomy*, 2010

- Kravtsov, A. V., Gnedin, O. Y., & Klypin, A. A. 2004, *ApJ*, 609, 482
- Kroupa, P., Tout, C. A., & Gilmore, G. 1993, *MNRAS*, 262, 545
- Larson, R. B. 1974, *MNRAS*, 169, 229
- Leitherer, C., Schaerer, D., Goldader, J. D., González Delgado, R. M., Robert, C., Kune, D. F., de Mello, D. F., Devost, D., & Heckman, T. M. 1999, *ApJS*, 123, 3
- Li, Y., Helmi, A., De Lucia, G., & Stoehr, F. 2009, *MNRAS*, 397, L87
- Lisenfeld, U. & Ferrara, A. 1998, *ApJ*, 496, 145
- Mac Low, M. & Ferrara, A. 1999, *ApJ*, 513, 142
- Macciò, A. V., Kang, X., & Moore, B. 2009, *ApJ*, 692, L109
- Mao, S., Jing, Y., Ostriker, J. P., & Weller, J. 2004, *ApJ*, 604, L5
- Marigo, P., Girardi, L., Bressan, A., Groenewegen, M. A. T., Silva, L., & Granato, G. L. 2008, *A&A*, 482, 883
- Martin, C. L. 1996, *ApJ*, 465, 680
- Marzke, R. O. & da Costa, L. N. 1997, *AJ*, 113, 185
- Mateo, M. L. 1998, *ARA&A*, 36, 435
- Mayer, L., Mastropietro, C., Wadsley, J., Stadel, J., & Moore, B. 2006, *MNRAS*, 369, 1021
- McGaugh, S. S. & Wolf, J. 2010, ArXiv e-prints

Moore, B., Ghigna, S., Governato, F., Lake, G., Quinn, T., Stadel, J., & Tozzi, P. 1999, *ApJ*, 524, L19

Muñoz, C. 2004, *International Journal of Modern Physics A*, 19, 3093

Mushotzky, R. F. 1983, NASA STI/Recon Technical Report N, 83, 33826

Navarro, J. F. & Steinmetz, M. 2000, *ApJ*, 528, 607

Neuschaefter, L. W., Im, M., Ratnatunga, K. U., Griffiths, R. E., & Casertano, S. 1997, *ApJ*, 480, 59

Okamoto, T. & Frenk, C. S. 2009, *MNRAS*, 399, L174

Okamoto, T., Frenk, C. S., Jenkins, A., & Theuns, T. 2009, ArXiv e-prints

Oort, J. H. 1940, *ApJ*, 91, 273

Ostriker, J. P., Peebles, P. J. E., & Yahil, A. 1974, *ApJ*, 193, L1

Pagels, H. & Primack, J. R. 1982, *Physical Review Letters*, 48, 223

Peñarrubia, J., McConnachie, A. W., & Navarro, J. F. 2008, *ApJ*, 672, 904

Penzias, A. A. & Wilson, R. W. 1965, *ApJ*, 142, 419

Press, W. H. & Schechter, P. 1974, *ApJ*, 187, 425

Quinn, T., Katz, N., & Efstathiou, G. 1996, *MNRAS*, 278, L49

Raiteri, C. M., Villata, M., & Navarro, J. F. 1996, *A&A*, 315, 105

Ratra, B. & Vogeley, M. S. 2008, *PASP*, 120, 235

Rauch, M. 1998, *ARA&A*, 36, 267

- Read, J. I., Pontzen, A. P., & Viel, M. 2006, MNRAS, 371, 885
- Rees, M. J. 1986, MNRAS, 218, 25P
- Rubin, V. C., Thonnard, N., & Ford, Jr., W. K. 1978, ApJ, 225, L107
- Sadoulet, B. 1999, Reviews of Modern Physics Supplement, 71, 197
- Sandage, A. & Binggeli, B. 1984, AJ, 89, 919
- Schirber, M. & Bullock, J. S. 2003, ApJ, 584, 110
- Shen, S., Wadsley, J., & Stinson, G. 2010, MNRAS, 1043
- Simon, J. D. & Geha, M. 2007, ApJ, 670, 313
- Skillman, E. D. 2007, in Groups of Galaxies in the Nearby Universe, ed. I. Saviane, V. D. Ivanov, & J. Borissova, 21–+
- Smith, S. 1936, ApJ, 83, 23
- Smoot, G. F., Bennett, C. L., Kogut, A., Wright, E. L., Aymon, J., Bogges, N. W., Cheng, E. S., de Amici, G., Gulkis, S., Hauser, M. G., Hinshaw, G., Jackson, P. D., Janssen, M., Kaita, E., Kelsall, T., Keegstra, P., Lineweaver, C., Loewenstein, K., Lubin, P., Mather, J., Meyer, S. S., Moseley, S. H., Murdock, T., Rokke, L., Silverberg, R. F., Tenorio, L., Weiss, R., & Wilkinson, D. T. 1992, ApJ, 396, L1
- Spergel, D. N., Bean, R., Doré, O., Nolta, M. R., Bennett, C. L., Dunkley, J., Hinshaw, G., Jarosik, N., Komatsu, E., Page, L., Peiris, H. V., Verde, L., et al. 2007, ApJS, 170, 377